SCIENCE CHINA Earth Sciences



•ARTICLE•

https://doi.org/10.1007/s11430-025-1668-1

Improve the forecast reliability of unusual tropical cyclone tracks using ensemble forecasts generated by O-CNOPs

Han ZHANG^{1,2,6}, Wansuo DUAN^{2*}, Yongjie HUANG³, Pak Wai CHAN⁴ & Stephane VANNITSEM⁵

Received April 9, 2025; revised August 4, 2025; accepted August 19, 2025; published online October 16, 2025

Abstract There exist significant challenges in accurately predicting unusual tropical cyclone (TC) tracks. This study applies the orthogonal conditional nonlinear optimal perturbations (O-CNOPs) method to the Weather Research and Forecast (WRF) model to improve ensemble forecast reliability of unusual TC tracks. Ensemble forecast experiments were conducted for twenty-three forecast periods of five TCs, all of which exhibited sharp turns, to examine the effectiveness of O-CNOPs. Results demonstrate that the O-CNOPs method outperforms the singular vectors (SVs) and bred vectors (BVs) methods by providing more stable and reliable improvements in TC track forecasting skills, from both deterministic and probabilistic perspectives. Notably, the O-CNOPs shows a superior ability to generate ensemble members that accurately predict the sharp turns of TCs at lead times from one to five days. These results highlight the superiority of the O-CNOPs method over the SVs and BVs methods in enhancing the forecasting accuracy of TC tracks, particularly for forecasting unusual TC tracks. This study underscores the potential of O-CNOPs to be extended to real-time TC forecasting and to play an important role in operational track forecasts.

Keywords Tropical cyclone, Ensemble forecast, Optimal perturbation

Citation: Zhang H, Duan W, Huang Y, Chan P W, Vannitsem S. 2025. Improve the forecast reliability of unusual tropical cyclone tracks using ensemble forecasts generated by O-CNOPs. Science China Earth Sciences, 68, https://doi.org/10.1007/s11430-025-1668-1

1. Introduction

Tropical cyclones (TCs) that occur over the western North Pacific (WNP) frequently bring extreme winds and heavy rainfall to China and pose significant threats to lives and property (Li and Zhao, 2022). The accuracy of TC-related wind and rainfall forecasts largely depends on the accuracy of TC track forecasts (Conroy et al., 2023; Qian et al., 2024).

Therefore, a precise TC track forecast is essential to mitigate the severe impacts of TC-related disasters.

Over the past few decades, significant advancements have been made in TC track forecasting. However, substantial challenges remain in both long-time forecasts of TC tracks and the prediction of unusual TC tracks. Long-time forecasting of abnormal TC tracks is particularly difficult (Zhang et al., 2018; Chen et al., 2020; Tang et al., 2021; Li et al., 2023; Liu et al., 2024). Notably, in recent years, the frequent occurrence of TCs with unusual tracks over the WNP has

¹ Henan Key Laboratory of Agrometeorological Support and Applied Technique, China Meteorological Administration (CMA), Zhengzhou 450003, China

² State Key Laboratory of Earth System Numerical Modeling and Application, Institute of Atmospheric Physics, Chinese Academy of Sciences, Beijing 100029, China

³ Center for Analysis and Prediction of Storms and School of Meteorology University of Oklahoma, Norman Oklahoma 73072, USA

⁴ Hong Kong Observatory, Hong Kong 999077, China

⁵ Royal Meteorological Institute of Belgium, Brussels 1180, Belgium

⁶ Henan Meteorological Observatory, Zhengzhou 450003, China

^{*} Corresponding author (email: duanws@lasg.iap.ac.cn)

posed even greater challenges to operational TC forecasts. For instance, most meteorological services failed to forecast the sharp northward turn of TC In-Fa (2021) three days before TC turning. Even when initialized at the time approaching the turn, some forecasting centers still missed the turn, resulting in track errors significantly exceeding the annual-mean track error for the year 2021 (Xiang et al., 2022; Liu et al., 2024). Similarly, during the early stages of TC Khanun (2023), the leading meteorological services, such as the European Centre for Medium-Range Weather Forecasts (ECMWF) and the US National Centers for Environmental Prediction (NCEP), consistently predicted that the storm would make landfall in China (Nie et al., 2025). However, the cyclone abruptly turned sharply northeastward, avoiding China entirely. It was then predicted to strike Japan but unexpectedly shifted northward again, ultimately making landfall in the Republic of Korea. Another example is TC Saola (2023). Most meteorological services did not accurately forecast the loop at the early stage of the TC, causing prominent errors in the predicted landfall location. These examples highlight that the long-time forecasts generally struggle to replicate the unusual TC tracks. Even when forecasts are initialized close to the time of turning, they still exhibit very large forecast uncertainties regarding TC tracks.

Ensemble forecasting has been widely adopted by Meteorological Departments to improve TC forecasting skill, provide the information of forecast uncertainty, and generate probabilistic forecasts (Puri et al., 2001; Dube et al., 2020). Advances in ensemble forecasting methods have significantly enhanced TC forecasting skill (Duan et al., 2018; Zhang et al., 2023). It is widely accepted that fast-growing initial perturbations, superimposed on control forecasts to represent initial uncertainties, are crucial for improving the reliability of ensemble forecasts (Toth and Kalnay, 1993, 1997; Palmer, 2019; Magnusson et al., 2019). Particularly, numerous studies have highlighted the role of environmental steering flows, which are sensitive to initial conditions, in modulating TC tracks (Yamaguchi and Majumdar, 2010; Wang and Ni, 2011; Miller and Zhang, 2019; Miyachi and Enomoto, 2021; Ma et al., 2022; Zhang et al., 2023). This sensitivity underscores the initial value problem of TC track forecasts. The ECMWF has adopted the singular vectors (SVs) method and the NCEP previously used the bred vectors (BVs) method to account for the initial uncertainties in TC track forecasting. Both methods aim to generate fastgrowing initial perturbations that replicate the forecast error growth and encompass the forecast uncertainties, achieving great success in improving TC track forecasting skill (Cheung and Chan, 1999; Cheung, 2001; Yamaguchi et al., 2009; Yamaguchi and Majumdar, 2010; Diaconescu and Laprise, 2012; Palmer, 2019). However, limitations remain. The BVs, responsible for growth behavior of initial perturbations prior to forecast initialization, often fail to maintain large growth rates during longer forecast lead times. This limitation frequently results in insufficient ensemble spreads to encompass the actual trajectory of the cyclones (Chan and Li, 2005; Lang et al., 2012; Thanh et al., 2016; Zhang et al., 2023). On the other hand, although SVs represent a group of fast-growing initial perturbations on control forecasts, they are derived from linearized dynamics of atmosphere motions and could possibly underestimate the forecast uncertainty when nonlinearities are playing an important role (Puri et al., 2001; Lang et al., 2012; Huo et al., 2019; Zhang et al., 2023).

Duan and Huo (2016) generalized SVs to the nonlinear regime and proposed the orthogonal conditional nonlinear optimal perturbations (O-CNOPs) method to fully account for the influence of nonlinearities. O-CNOPs represent a set of mutually orthogonal initial perturbations that have the maximum nonlinear evolution in their respective subspaces within a finite time interval (Duan and Huo, 2016; Huo et al., 2019; Zhang et al., 2023). Duan and Huo (2016) adopted a simple Lorenz-96 model (Lorenz, 1996) to address the dynamic rationality of the O-CNOPs and showed a significantly higher ensemble forecasting skill for the O-CNOPs than that of the SVs. Furthermore, Huo et al. (2019) extended the O-CNOPs to TC track ensemble forecasting using the fifth-generation Pennsylvania State University, National Center for Atmospheric Research Mesoscale Model (MM5) and showed clear advantages of O-CNOPs over methods based on random perturbations (RPs), BVs, and SVs. Although the MM5 model is generally considered less advanced and performs poorly in TC track simulations compared to the Weather Research and Forecasting (WRF) model (Pattanayak and Mohanty, 2008), subsequent studies reaffirmed the strength of O-CNOPs. Zhang et al. (2023) applied the O-CNOPs to TC track ensemble forecasting using the WRF model and found that the method consistently outperformed both the SVs and BVs methods, demonstrating superior deterministic and probabilistic forecasting skill. These findings underscore the significant potential of O-CNOPs for further improving TC track forecasting accuracy, making it a promising tool for operational meteorological applications.

As discussed above, long-time forecasts of unusual TC tracks remain particularly challenging, and so far, the capability of O-CNOPs in forecasting such unusual tracks has not been systematically evaluated. This raises a key question: can the O-CNOPs method greatly improve the accuracy of forecasting unusual TC tracks? To address this, the present study employs the O-CNOPs method to conduct ensemble forecasting experiments particularly for unusual TC tracks using the WRF model.

The rest of the paper is organized as follows. Section 2 describes the O-CNOPs method. Section 3 provides an overview of the TC cases with unusual tracks adopted in this study, along with an evaluation of the ensemble forecasting

performance achieved using the O-CNOPs, SVs, and BVs methods, and then details why the O-CNOPs is prone to capture the sharp turns of TC tracks. Finally, Section 4 provides the summary and discussion.

2. The O-CNOPs method and associated numerical model

In this study, we employ the O-CNOPs method within the WRFV3.6 model (Skamarock et al., 2008) to generate ensemble members for forecasting unusual TC tracks. Although our previous study (Zhang et al., 2023) also utilized WRFV3.6 and O-CNOPs for TC track forecasts, its focus was not on unusual tracks. Building on that, we continue to use WRFV3.6 but apply the O-CNOPs approach in a different manner, specifically tailored to forecasting unusual TC tracks. To avoid redundancy, we do not elaborate on the WRFV3.6 model here, as its details can be found in Zhang et al. (2023). Instead, we only present the specifics of our O-CNOPs implementation below.

The O-CNOPs, denoted as \mathbf{x}_{0j}^* (j=1, 2, 3, ...), constitute a set of distinct initial perturbations that are mutually orthogonal and exhibit maximal nonlinear growth within a predefined time interval $[0, \tau]$, referred to as the "optimization time interval" (OTI; see Zhang et al., 2023), in their respective constrained subspaces Ω_j (Duan and Huo, 2016). The jth CNOP is obtained by solving the optimization problem given in eq. (1).

$$\mathbf{J}(\mathbf{x}_{0j}^{*}) = \max_{\mathbf{x}_{0j} \in \Omega_{j}} \left[PM_{\tau}(\mathbf{X}_{0} + \mathbf{x}_{0j}) - PM_{\tau}(\mathbf{X}_{0}) \right]^{\mathrm{T}} \times \mathbf{C}_{2} \left[PM_{\tau}(\mathbf{X}_{0} + \mathbf{x}_{0j}) - PM_{\tau}(\mathbf{X}_{0}) \right], \tag{1}$$

The subspace Ω_i is represented by

$$\begin{cases}
\left\{\mathbf{x}_{0j} \in \mathbf{R}^{n} \middle| \mathbf{x}_{0j}^{\mathsf{T}} \mathbf{C}_{1} \mathbf{x}_{0j} \leq \delta \right\}, & j = 1, \\
\left\{\mathbf{x}_{0j} \in \mathbf{R}^{n} \middle| \mathbf{x}_{0j}^{\mathsf{T}} \mathbf{C}_{1} \mathbf{x}_{0j} \leq \delta, \mathbf{x}_{0j} \perp \Omega_{k}, k = 1, \dots, j - 1 \right\}, & j > 1
\end{cases}$$
(2)

where $\mathbf{X}_0 \in \mathbb{R}^n$ represents the state vector, and M denotes the nonlinear propagator of the numerical forecast model. The superscript "T" indicates a transpose, and δ is a positive value defining the maximum allowable amplitude of the initial perturbation. The operator P serves as a local projection, taking a value of 1 when the final perturbations fall within the "verification region" (i.e., the region of interest for forecast accuracy) and 0 otherwise. In the current study, the verification region is defined as a fixed $10^{\circ} \times 10^{\circ}$ box centered on the TC position at the optimization time, a choice made to isolate the properties of the uncertainties in the TC

circulation at this time (Tseng and Lai, 2020), while the initial perturbations are generated over the entire model domain. In eqs. (1) and (2), both C_1 and C_2 adopt the total moist energy and are expressed by eq. (3).

$$\|\delta \mathbf{X}\|_{C_1}^2 = \|\delta \mathbf{X}\|_{C_2}^2$$

$$= \frac{1}{D} \int_{D} \int_{0}^{1} \left[\mathbf{u}'^2 + \mathbf{v}'^2 + \left(\frac{g}{\overline{N} \, \overline{\theta}} \right)^2 \mathbf{\theta}'^2 + R_{\mathbf{a}} T_{\mathbf{r}} \left(\frac{\mathbf{p}'_s}{p_{\mathbf{r}}} \right)^2 + \frac{L^2}{c_p T_r} \mathbf{q}'^2 \right] d\sigma dD.$$
(3)

The eq. (3) involves the zonal wind perturbation (u'), meridional wind perturbation (v'), potential temperature perturbation (θ '), surface pressure perturbation (\mathbf{p}'_s), and water vapor mixing ratio perturbation (\mathbf{q} '). It also prescribes the physical reference temperatures $\overline{\theta}$ =300 K, T_r =270 K, and pressure p_r =1000 hPa. In eq. (3), g represents the gravitational acceleration, R_a and c_p are the dry air gas constant and the constant-pressure specific heat of dry air, while \overline{N} and L denote the Brunt-Vaisala frequency and the latent heat of condensation per unit mass, respectively. The vertical integrations of the kinetic and potential energy terms, associated with \mathbf{u}' , \mathbf{v}' , $\mathbf{\theta}'$ and \mathbf{p}'_s , extend up to the top level, while the water vapor term \mathbf{q}' is limited to below 500 hPa.

Referring to Zhang et al. (2023), we choose the OTI=6 h, initial perturbation amplitude δ =1.8, and ensemble size N=21, for which the O-CNOPs ensemble achieves the highest ensemble forecasting skill for TC tracks. In this study, we still adopt the Spectral Projected Gradient 2 method (Birgin et al., 2000), as used in Zhang et al. (2023), to solve the optimization problem given by eq. (1) and compute the O-CNOPs. Since unusual TC motion may be influenced by multi-scale interactions, we employ a model domain with an increased resolution of 30 km horizontally and 31 vertical levels, extending from the surface to the top of the atmosphere at 50 hPa, for ensemble forecasting experiments in this study. In contrast to the approach used in Zhang et al. (2023), where O-CNOPs are calculated at a horizontal resolution of 60 km and 15 vertical levels, followed by ensemble forecasts at the same resolution, the present study first calculates the O-CNOPs at this coarser resolution and then linearly interpolates them to a higher resolution of 30 km horizontally and 31 vertical levels. The interpolated O-CNOPs are subsequently used to construct the initial perturbations for the actual ensemble forecasts. The ensemble size N=21 mentioned above requires 10 such initial perturbations. These initial perturbations, along with their negative counterparts, are then superimposed onto the initial field of the control forecast to generate 20 perturbed initial fields, with the control forecast utilizing the Global Forecast System (GFS) at 1.0°×1.0° resolution and 6-hour intervals to provide the initial and boundary conditions. The WRFV3.6 model with higher resolution is then integrated to generate 20 perturbed forecasts, which, along with the control forecast,

constitute 21 ensemble members for each case.

To assess the performance, the O-CNOPs ensemble forecasts are compared with those generated using traditional methods, including the SVs method implemented in the ECMWF and the BVs method previously used by NCEP. The configurations for both the SVs and BVs are identical to those employed in Zhang et al. (2023), where it was shown that O-CNOPs achieves higher forecasting skill than both SVs and BVs under various configurations. A brief overview of the SVs and BVs methods was provided in Appendix A of Zhang et al. (2023).

3. Ensemble forecasts for unusual TC tracks

In this section, we first describe the TCs with unusual tracks, and then assess the ability of O-CNOPs to improve the ensemble forecasting skill of unusual tracks compared with SVs and BVs.

3.1 Cases overview

To explore the ensemble forecasts of unusual tracks, it is necessary to distinguish unusual TC tracks from typical ones. However, a universally accepted definition of sudden TC track changes has not yet been established (Li et al., 2023). In

operational forecasting in China, thresholds of a 45° right deflection or a 30° left deflection within 12 h are commonly used to identify unusual TC tracks. These criteria have also been used in previous studies, such as Gong et al. (2018). Interestingly, Dai et al. (2014) provided the rationale behind the above criteria, illustrating that in the WNP, the occurrence probability of a right deflection exceeding 45° within 12 h is less than 2.8% and that of a left deflection exceeding 30° is less than 8.7%. These criteria effectively identify sharp turning tracks, distinguishing them from gradually recurving ones. Besides, we do not consider the short fluctuations around a relatively smooth track, so the TC's movements should be relatively stable after passing the turning point. Based on these criteria, we select three TCs exhibiting unusual tracks (i.e., Hinnamnor (2022), Khanun (2023), Saola (2023)) from 2022 to 2023. Additionally, Megi (2010) and Tembin (2012), previously analyzed in Zhang et al. (2023) without a focus on unusual tracks, also satisfy these criteria and are included in this study. All five TCs had significant impacts on China.

The tracks of these five TCs are shown in Figure 1, which highlights six sharp turning points (as marked by red stars). Both Megi (2010) and Hinnamnor (2022) underwent an abrupt northward turn, while Khanun (2023) followed a zigzagging track with a sharp northeastward turn on 4 August 2023 and another abrupt northward turn on 7 August

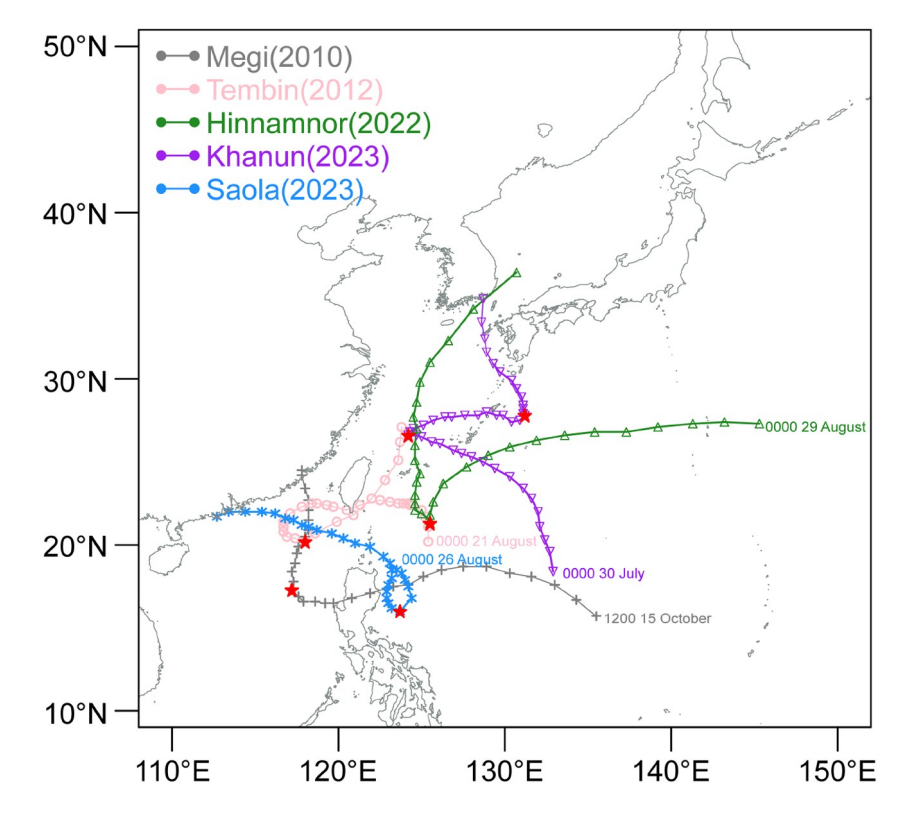


Figure 1 Best tracks of the five selected TCs(i.e., Megi (2010), Tembin (2012), Hinnamnor (2022), Khanun (2023), Saola (2023)) as obtained from the China Meteorological Administration (CMA). The starting points of each track correspond to their first initialized times, with subsequent tracks marked at 6-h intervals. The red stars denote six unusual turning points of the five TC case.

2023. Meanwhile, Tembin (2012) and Saola (2023) exhibited counterclockwise looping tracks. For the five TC cases, a total of eighteen forecast periods, detailed in Table 1, span between five and ten days, depending on each TC's lifetime. Since Khanun (2023) experienced two abrupt turns during its forecast periods, there are twenty-three ensemble forecast experiments for the six turning points.

3.2 Evaluation of ensemble forecasts for sharp TC turns

We conduct twenty-three ensemble forecast experiments for the six turning points of the five TCs, following the methodology outlined in section 2. Each forecast has 21 ensemble members, resulting in a total of 483 ensemble members generated for each method, i.e., the O-CNOPs, SVs, and BVs. Utilizing these ensemble members, we evaluate the probability of accurately capturing the sharp turns of the TCs. Additionally, the performance of ensemble mean forecast is also evaluated by quantifying the track errors during the turning stages. The results are analyzed and compared among the three methods.

Figures 2–4 show the control forecasts and the corresponding ensemble forecasts using BVs, SVs and O-CNOPs. The results reveal that the control forecasts significantly

deviate from the best track, especially when initialized well before the TC turning timing. These forecasts frequently fail to accurately capture the timing, location, and angle of the TC turn. In this case, effective ensemble forecasts should adequately represent the uncertainty, allowing the true TC track to fall within the ensemble spread. However, as shown in Figures 2-4, the ensemble members made by BVs and SVs tend to closely cluster around the control forecasts, while the best tracks often fall outside the ensemble spread, particularly for longer lead times. Differently, O-CNOPs can provide more ensemble members that obviously deviate from the corresponding control forecasts and often exhibit a broader spread to cover the best tracks. Statistically, among the twenty-three forecasts, eighteen forecasts using O-CNOPs successfully span the best track with their turning locations, timing, and angles, while only five forecasts using SVs and four forecasts using BVs achieve this outcome (see Table 1). This implies that the O-CNOPs method has a significantly higher probability of capturing the sharp TC turns in forecasts compared to the SVs and BVs.

Now we quantify the probabilities of the ensemble members made by O-CNOPs capturing the sharp turn of TCs, including their turning location, timing, and angle. Such probabilistic assessments in real-world forecasts can provide useful warning information for decision-makers. To address

Table 1 Forecast periods (UTC) for each TC^{a)}

TC names	Forecast periods (UTC)	O-Cì	NOPs	S	√s	ву	/s
Megi	12:00 15 October 2010 to 12:00 23 October 2010	√ ×		<	×		
	12:00 16 October 2010 to 12:00 23 October 2010	\checkmark		×		×	
	12:00 17 October 2010 to 12:00 23 October 2010	$\sqrt{}$		\checkmark		×	
	12:00 18 October 2010 to 12:00 23 October 2010	\checkmark		$\sqrt{}$		$\sqrt{}$	
Tembin	00:00 21 August 2012 to 00:00 29 August 2012	√ ×		<	×		
	00:00 22 August 2012 to 00:00 29 August 2012	×		×		×	
	00:00 23 August 2012 to 00:00 29 August 2012	$\sqrt{}$				$\sqrt{}$	
	00:00 29 August 2022 to 00:00 06 September 2022	>	×	×		×	
***	00:00 30 August 2022 to 00:00 06 September 2022	\checkmark		×		×	
Hinnamnor	00:00 31 August 2022 to 00:00 06 September 2022	\checkmark		\checkmark		$\sqrt{}$	
	00:00 01 September 2022 to 00:00 06 September 2022	$\sqrt{}$		×		×	
	00:00 30 July 2023 to 00:00 09 August 2023	$\sqrt{}$	×	×	×	×	×
	00:00 31 July 2023 to 00:00 10 August 2023	$\sqrt{}$	$\sqrt{}$	×	×	×	×
Khanun	00:00 01 August 2023 to 00:00 10 August 2023	$\sqrt{}$	×	×	×	×	×
	00:00 02 August 2023 to 00:00 10 August 2023	$\sqrt{}$	$\sqrt{}$	×	×	×	×
	00:00 03 August 2023 to 00:00 10 August 2023	$\sqrt{}$	$\sqrt{}$	$\sqrt{}$	×	$\sqrt{}$	×
C1-	00:00 26 August 2023 to 00:00 02 September 2023	×		×		×	
Saola	00:00 27 August 2023 to 00:00 02 September 2023	\checkmark		×		×	

a) Check marks ($\sqrt{}$) indicate that the ensemble members for the O-CNOPs, SVs or BVs successfully encompass the best track including the turning location, time, and angle. Cross marks (\times) indicate that the ensemble members fail to span these key turning features.

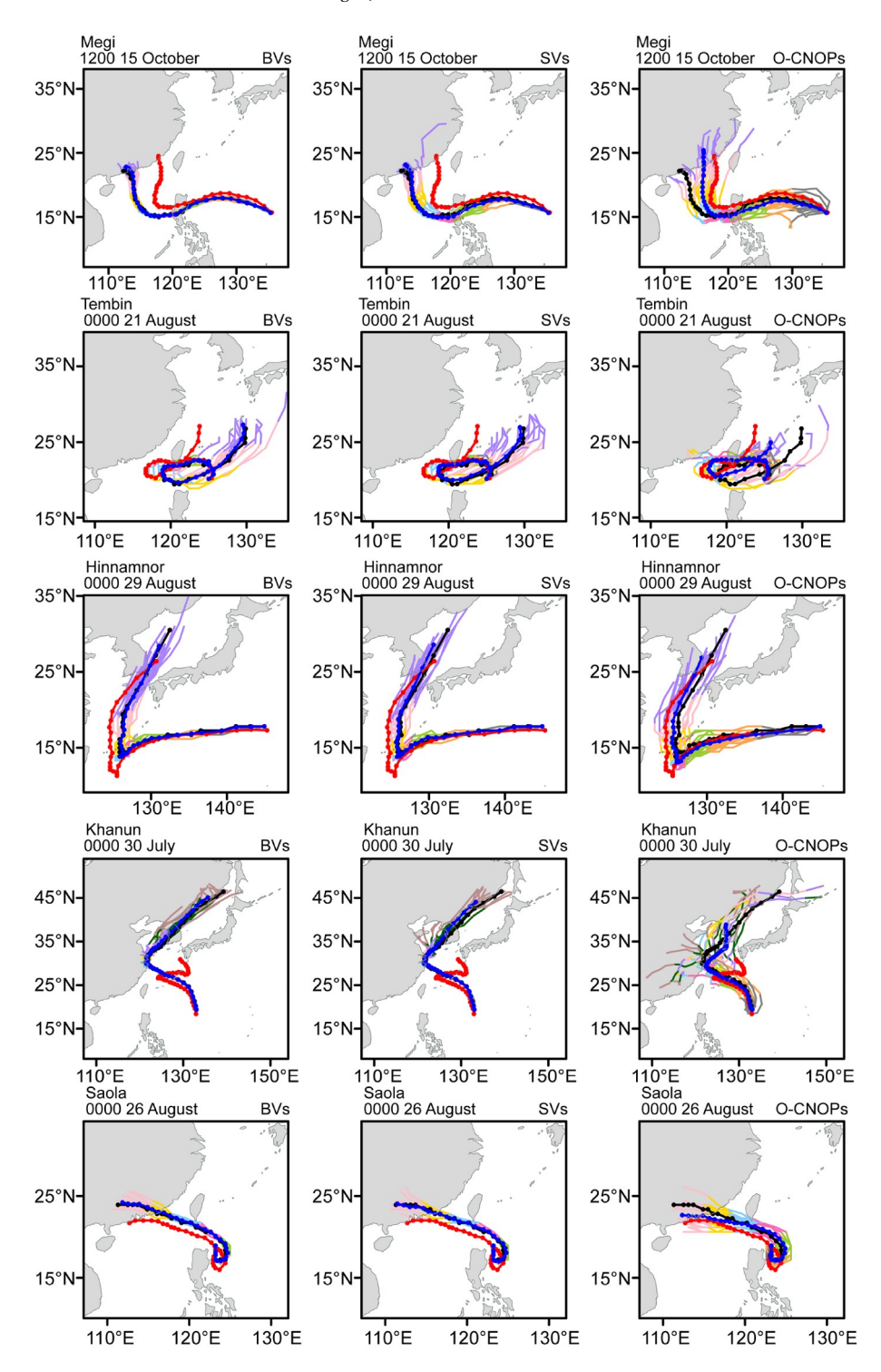


Figure 2 The ensemble forecasts of TC tracks during the first forecast periods of Megi (2010), Tembin (2012), Hinnamnor (2022), Khanun (2023) and Saola (2023) generated by the BVs (left column), SVs (middle column), and O-CNOPs (right column). Here are the best tracks (red lines), control forecasts (black lines), ensemble mean forecasts (blue lines) and the ensemble member forecasts. Time phases marked with different colors represent 0–24 h (gray lines), 24–48 h (orange lines), 48–72 h (green lines), 72–96 h (magenta lines), 96–120 h (light blue lines), 120–144 h (yellow lines), 144–168 h (pink lines) and 168–192 h (purple lines), 192–216 h (dark green lines), and 216–240 h (brown lines).

this question, we define allowable error bounds for forecast accuracy in predicting the sharp turn components (turning location, time, and angle). This unusual approach has been designed since there is no standardized metric for TC turning

forecast accuracy. The different combinations of error bounds in Table 2 produce a total of twenty-seven categories of distinct degrees of accuracy for evaluating TC turning forecasts. In Figure 5, the percentage of the number of en-

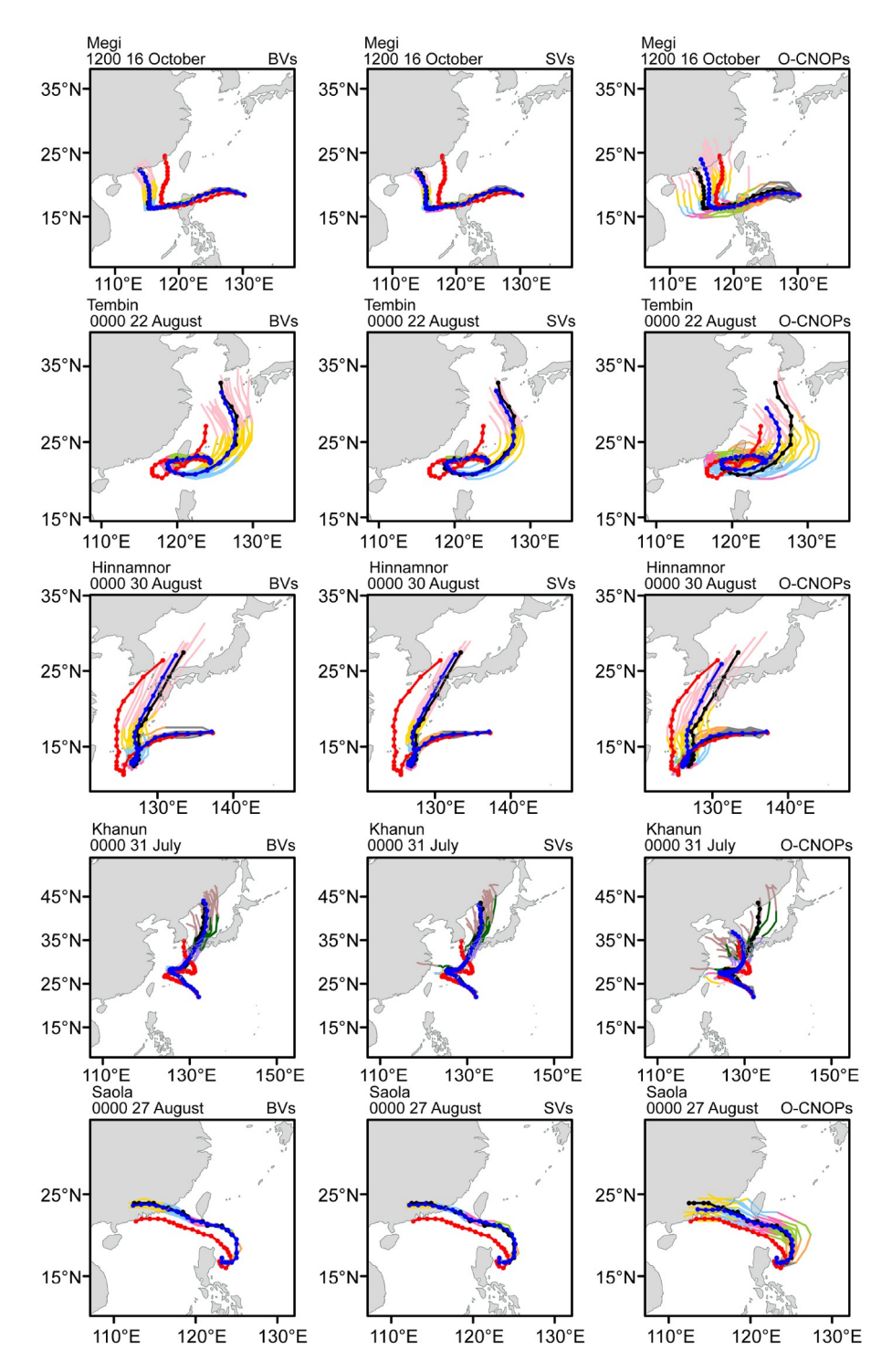


Figure 3 Same as Figure 2, but for the tracks in the second forecast periods of Megi (2010), Tembin (2012), Hinnamnor (2022), Khanun (2023) and Saola (2023).

semble members that capture the sharp TC turns among the 483 members generated from the 23 forecast experiments is plotted for each kind of degree of accuracy. It is shown that, across all degrees of accuracy, the percentages achieved by the O-CNOPs method, i.e. 10%–63%, are consistently and significantly higher than those obtained using SVs and BVs,

i.e. 3%–38% and 2%–33%. It highlights the potential of O-CNOPs to provide more ensemble members that better capture the sharp turns of TCs and provide more reliable probabilistic information regarding the occurrence of sharp turns, which could enhance forecast guidance and decision-making.

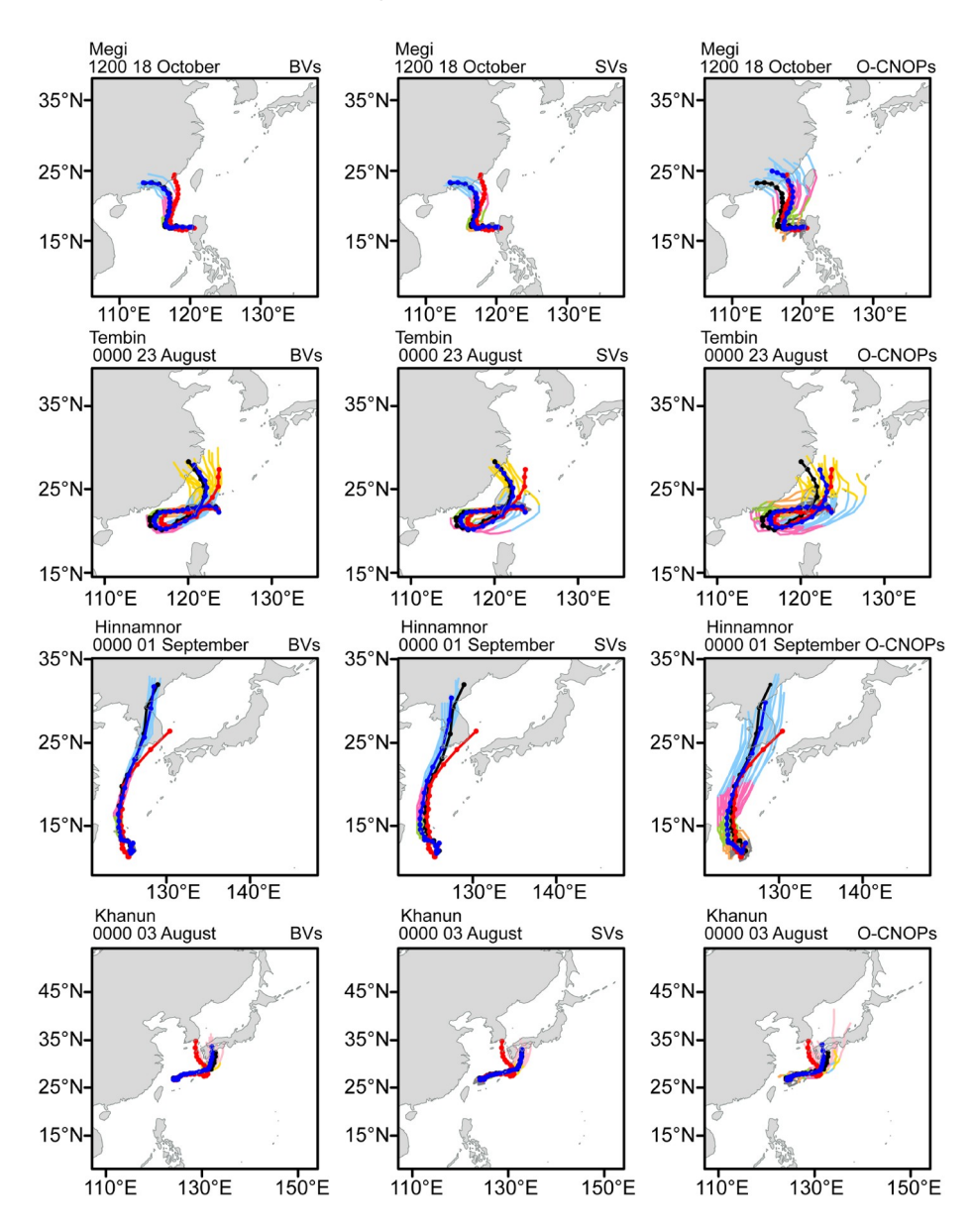


Figure 4 Same as Figure 2, but for the tracks in the last forecast periods of Megi (2010), Tembin (2012), Hinnamnor (2022) and Khanun (2023).

Figure 6 further provides the percentage of ensemble members that capture the sharp turn among the total ensemble members at lead times of 24, 48, 72, 96, and 120 h. These calculations assume allowable error bounds of 120 km for turning location, 12 hours for turning time, and 10° for turning angle. Note that the control forecasts of five TCs often only capture the turning time and location within the above allowable degree of accuracy for lead times of 1–2 days, but fail to accurately forecast the angle of deflection (see Figure 4). In contrast, from Figure 6, it is evident that the O-CNOPs produces more members capable of reproducing the sharp turn 1 to 5 days in advance compared to the SVs and BVs. Specifically, at lead times from 1 to 3 days, more than 50% of O-CNOPs ensemble members capture the sharp turns of these TCs. At a lead time of 4 days, nearly 50% of

the O-CNOPs ensemble members succeed, and at a lead time of 5 days, more than 30% of the O-CNOPs ensemble members still capture the sharp turns. For the BVs and SVs, however, only at lead times of 1 and 2 days do more than 50% of the ensemble members successfully capture the sharp turns. Beyond 3 days, the percentages drop sharply, with less than 10% of ensemble members capturing the sharp turn at lead times of 4 and 5 days. This limitation significantly reduces their ability to provide advanced warning for TC track changes. Taking Khanun (2023) as an example, when initialized at five days prior to its first sharp turn, the control forecast and all members for the BVs and SVs erroneously predicted landfall along the southeastern coast of China. However, about 30% of the ensemble members for the O-CNOPs successfully predicted its sharp northeastward turn

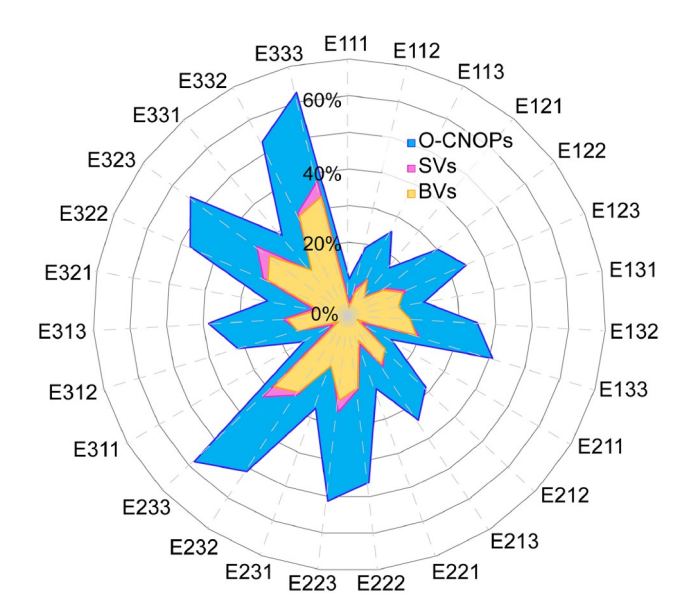


Figure 5 The percent of the number of the ensemble members capturing the TC turns among the total number of ensemble members for the twenty-three forecast periods (so a total of 483 forecasts). Yellow is for BVs, purple is for SVs, and blue is for O-CNOPs. The notation Eijk (i=1, 2, 3; j=1, 2, 3; k=1, 2, 3) represents the category of the degrees of accuracy provided by ith error bound for turning location, jth error bound for turning time, and kth error bound for turning angle in Table 2.

Table 2 Error bounds for the forecast accuracy in predicting the timing, location, and angle of TC turn.

Error bounds	Turning location	Turing time	Turning angle		
1	60 km	6 h	5°		
2	120 km	12 h	10°		
3	180 km	18 h	15°		

(see Figure 2). Therefore, the O-CNOPs demonstrates a superior ability to generate more members that successfully predict the sharp turns of TCs at longer lead times, thereby offering more valuable warning information on the sudden changes of TC tracks.

We further quantify the deterministic skill of ensemble mean forecasts made by BVs, SVs, and O-CNOPs in forecasting the sharp turns of the TC tracks. Firstly, we compare the forecast errors of turning location and time among the control forecasts and three ensemble mean forecasts. As shown in Figure 7, the forecast errors of the turning location and time for the O-CNOPs ensemble mean forecast (152 km, 8 h) are smaller than those of the control forecast (225 km, 11 h). Particularly, O-CNOPs exhibit clear advantage over BVs and SVs in reducing large forecast errors related to the turning position and turning time. Although O-CNOPs show higher probabilistic skill in capturing the turning angle, the ensemble mean generated by O-CNOPs, as well as those for BVs and SVs, performs worse than the control forecast in forecasting the turning angle within 12 h. The sharp turning angles within 12 h of the ensemble mean forecasts are overly

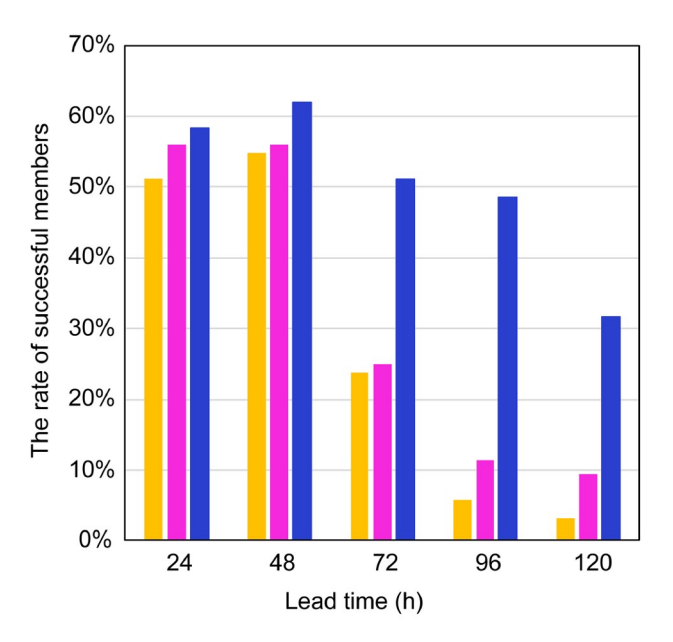


Figure 6 The percentage of ensemble members successfully capturing the TC sharp turns relative among the total number of ensemble members generated by O-CNOPs (blue), the SVs (purple), and the BVs (yellow) at different lead times when the degree of accuracy is prescribed by the following error bounds: 120 km for turning location, 12 h for turning timing, and 10° for turning angle.

smoothed compared to each individual ensemble member due to filtering effects (see Figures 2-4). From another perspective, Qian and Mao (2023) computed the track errors during the turning stages to evaluate the forecasting skill for the sharp turns of the TC tracks. Building upon this approach, we also examine the ensemble mean forecast errors for TC tracks during the turning stages, starting 24 hours before and ending 24 hours after the turning time. The ensemble mean forecast errors of the twenty-three forecasts. together with the control forecasts, are presented in Figure 8 using box-whisker plots. It is shown that the track errors of control forecasts gradually increase as TCs approach their turning points. Ensemble mean forecasts for the BVs and SVs provide only minor improvements over the control forecasts, with error reduction rates of less than 3%. Notably, the ensemble mean forecasts using O-CNOPs significantly decrease track errors during sharp turns across all three quantiles (25th, 50th and 75th). Specifically, the O-CNOPs ensemble mean forecasts reduce the track errors of the control forecasts by over 29% on average across all twentythree forecasts. For control forecasts with errors in the upper quartile (indicating relatively large track errors), O-CNOPs achieve error reductions exceeding 34%, whereas the reductions for SVs and BVs are less than 2%. Furthermore, the smallest interquartile range, defined as the difference between 25th and 75th quantiles, demonstrates that the O-CNOPs method provides more stable and consistent improvement to the control forecasts compared to the SVs and BVs methods.

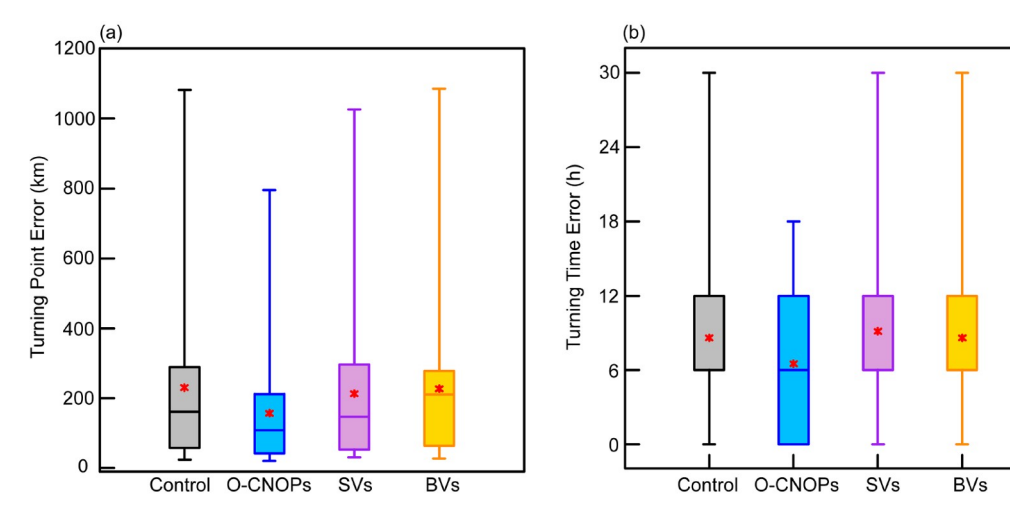


Figure 7 Box plots of the turning point errors (a) and turning time errors (b) for the twenty-three forecasts in the control forecasts (black) and ensemble mean forecasts using BVs (yellow), SVs (purple), and O-CNOPs (blue). The red points represent the mean values and the boxes show the 25th, 50th and 75th percentiles. The top and bottom lines indicate the largest and smallest values excluding outliers.

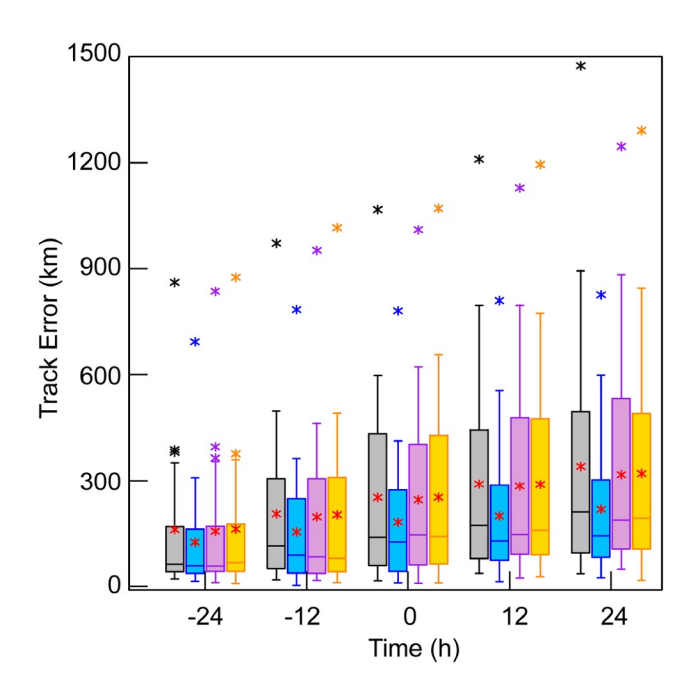


Figure 8 Box plots of track errors for the twenty-three forecasts during TC turning stage (defined as 24 h before to 24 h after the turning time) in the control forecasts (black) and ensemble mean forecasts using BVs (yellow), SVs (purple), and O-CNOPs (blue). The red points represent the mean values, the other points are the outliers, and the boxes show the 25th, 50th and 75th percentiles. The top and bottom lines indicate the largest and smallest values excluding outliers.

3.3 Explaining why the O-CNOPs ensemble members are more prone to capture TC sharp turn

Among the eighteen forecast periods in Table 1, the control forecast of Khanun (2023) has the largest track errors during its first forecast period, which was initialized at 00:00 UTC on 30 July 2023 (approximately 5 days prior to its sharp northeastward turn). As stated in Section 1, this sharp

northeastward turn of Khanun (2023) also posed great challenges to operational forecasts. For such a difficult forecast case, only O-CNOPs ensemble is capable of generating ensemble members that noticeably deviate from the corresponding control forecasts and exhibit a broader spread to encompass the best track, thereby achieving better forecast reliability (see Figure 2). In the rest of this section, we take the forecast of Khanun (2023) initialized at 00:00 UTC on 30 July 2023 as an example to illustrate why O-CNOPs are more prone to generate ensemble members that capture the sharp northeastward turn of Khanun (2023), whereas both SVs and BVs fail to do so.

The perturbed total moist energies (TMEs) differ in vertical structures among the three methods (see Figure 9). The initial TMEs for BVs exhibit the largest magnitudes at the upper layers above 300 hPa, and the TMEs for SVs have the largest magnitudes in the low level below 800 hPa, while O-CNOPs have the largest TMEs in the middle to lower pressure levels, as illustrated in Zhang et al. (2023). Actually, the initial uncertainties in the middle to lower troposphere can lead to large forecast uncertainties of TC tracks (Wang and Ni, 2011; Torn et al., 2018). Notably, O-CNOPs are unique in effectively capturing this critical sensitivity. As a result, the sensitivity of O-CNOPs promotes a more significant amplification of TMEs across all vertical layers compared to SVs and BVs (see Figure 9). Consequently, O-CNOPs are more prone to generate ensemble members able to diverge more from the control forecast, which misses the sharp northeastward turn of Khanun (2023), thus producing a larger ensemble spread that has a superior ability to capture sharp turns of TC tracks (see Figure 2).

Figure 10 shows the horizontal structures for the first three BVs, SVs and O-CNOPs, along with the 500 hPa geopotential height and steering flow for the control forecast at the

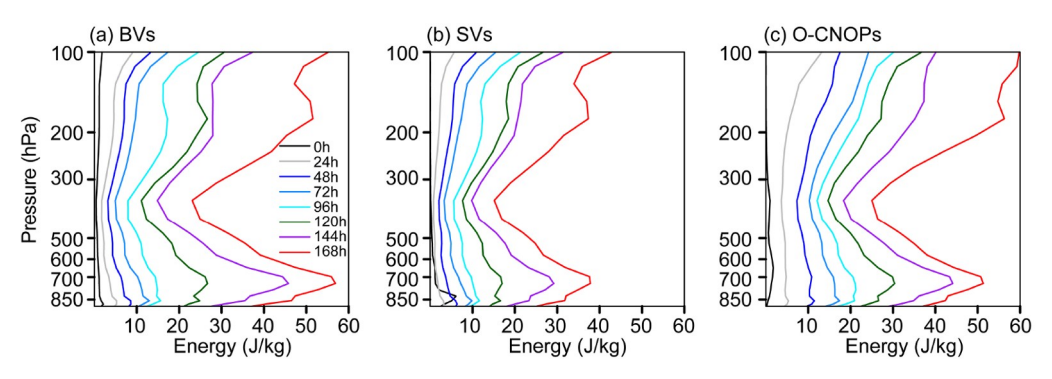


Figure 9 When initialized at 00:00 UTC on 30 July 2023 for TC Khanun (2023), vertical profiles of the TMEs (unit: J/kg) averaged over the entire analysis domain and across all ensemble members respectively generated by (a) BVs, (b) SVs and (c) O-CNOPs at the initial time (black curves) and at the lead times of 24 to 168 h (colored curves).

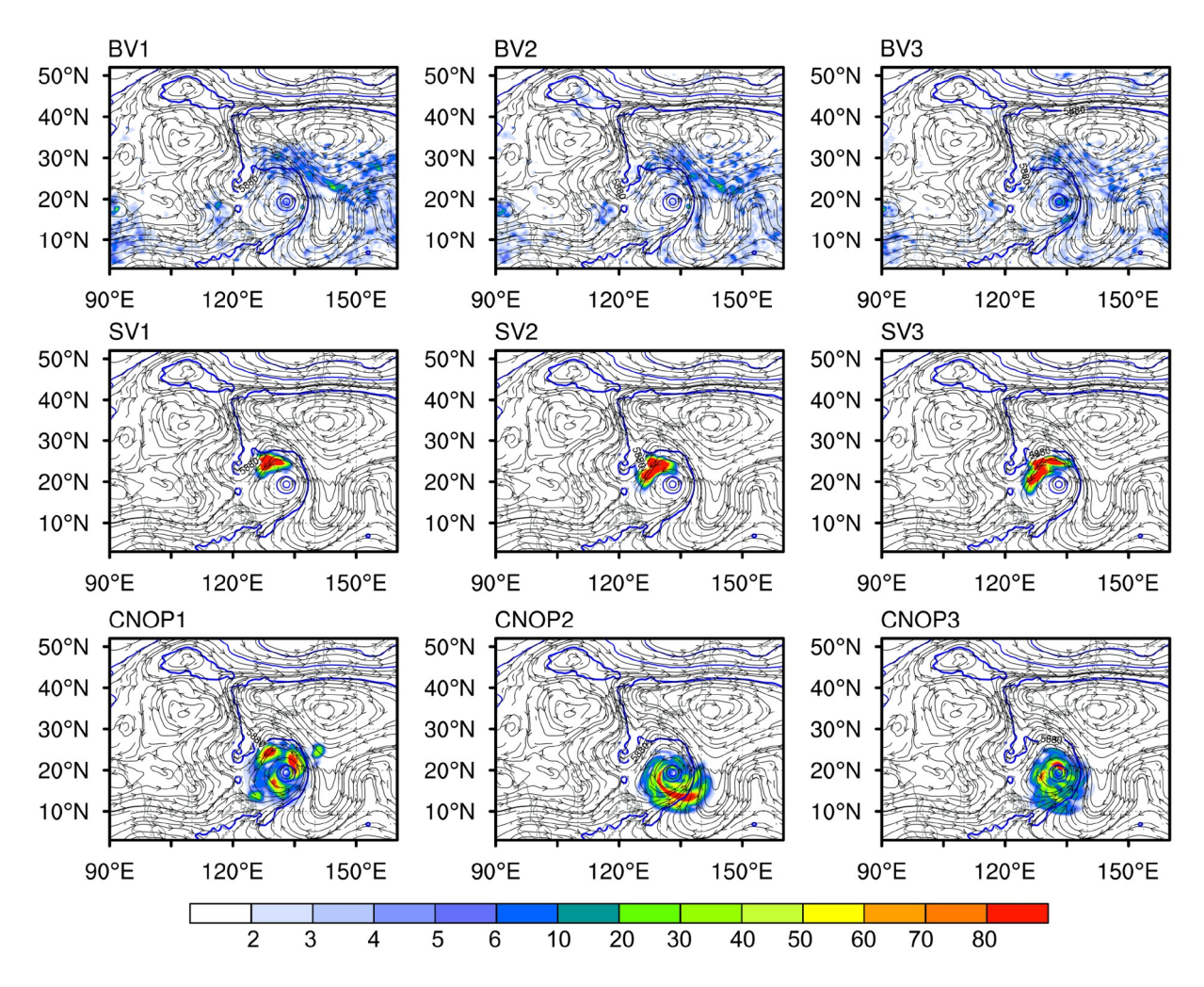


Figure 10 Horizontal structures of vertically averaged TMEs (shading; unit: J/kg) for the first three BVs, SVs and O-CNOPs. The blue contours and black streamlines show the 500 hPa geopotential heights (unit: gpm) and deep-layer (from 250 to 850 hPa) mean winds (unit: m/s).

initial time. It is known that Khanun (2023) initially moves northwestward due to the southeasterly steering flow associated with the western Pacific subtropical high (WPSH) and the subsequent unusual movement of Khanun (2023) is determined by the intensity and location changes of the WPSH (Chen et al., 2024). As is visible in Figure 10, the TMEs for

BVs are scattered around the TC and its associated largescale flows, while both SVs and CNOPs concentrate their TMEs in the confluence regions of the circulations represented by WPSH and Khanun (2023). However, their energy distributions differ: the SVs place their TMEs to the northwest of Khanun (2023), while O-CNOPs form a halfannulus distribution around Khanun (2023). Both of them reflect the influence of WPSH on the TC, but the O-CNOPs ensemble provides a much larger spread than the SVs ensemble (and also the BVs ensemble) in the vicinity of Khanun (2023) and its surrounding steering flow at the initial stage (see Figure 11a). This broader spread is attributed to the fully nonlinear optimal growth nature of O-CNOPs. This would contribute to much larger alterations in the location and structure of Khanun (2023), which interact dynamically with the WPSH and further influence its intensity and location, in turn modulating the movement of the TC.

Figure 12 shows the 5880-gpm contour at 500 hPa for the three ensembles, outlining the structures of WPSH. The O-CNOPs ensemble displays much larger diversity in the intensity and location of WPSH (see Figure 12a), representing its larger uncertainties, especially as the forecast approaches the northeastward turn of Khanun (2023). This enhanced spread of WPSH is accompanied by a broader range of steering flows along its edge (see Figure 11a), which is critical in determining the TC's northeastward turn. As a result, the O-CNOPs ensemble generates substantial variability in the turning location and angle of its members (see Figure 2).

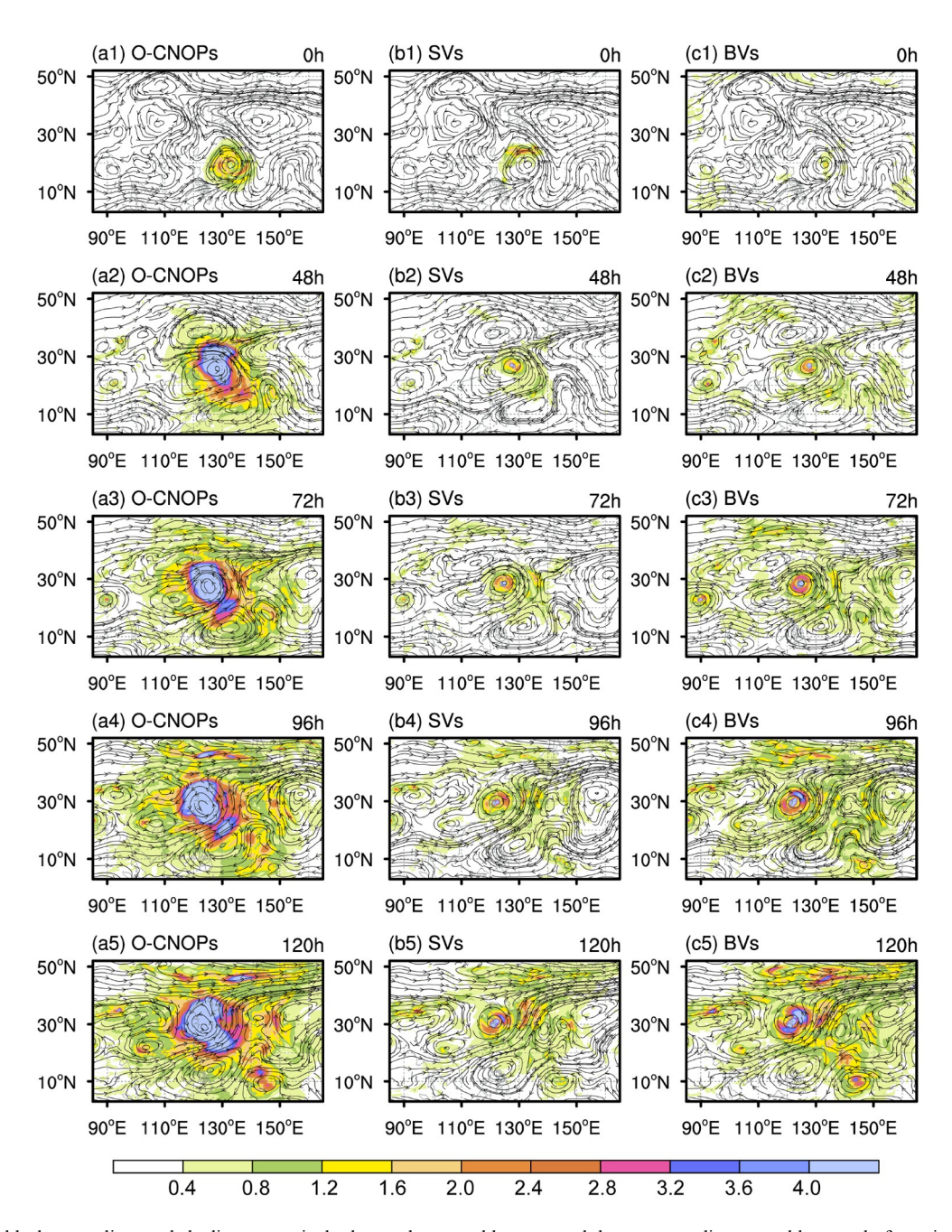


Figure 11 The black streamlines and shading respectively denote the ensemble mean and the corresponding ensemble spread of steering flow (unit: m/s) made by the O-CNOPs (a1-a5), SVs (b1-b5), and BVs (c1-c5) at the initial time and at the lead times of 48 to 120 h.

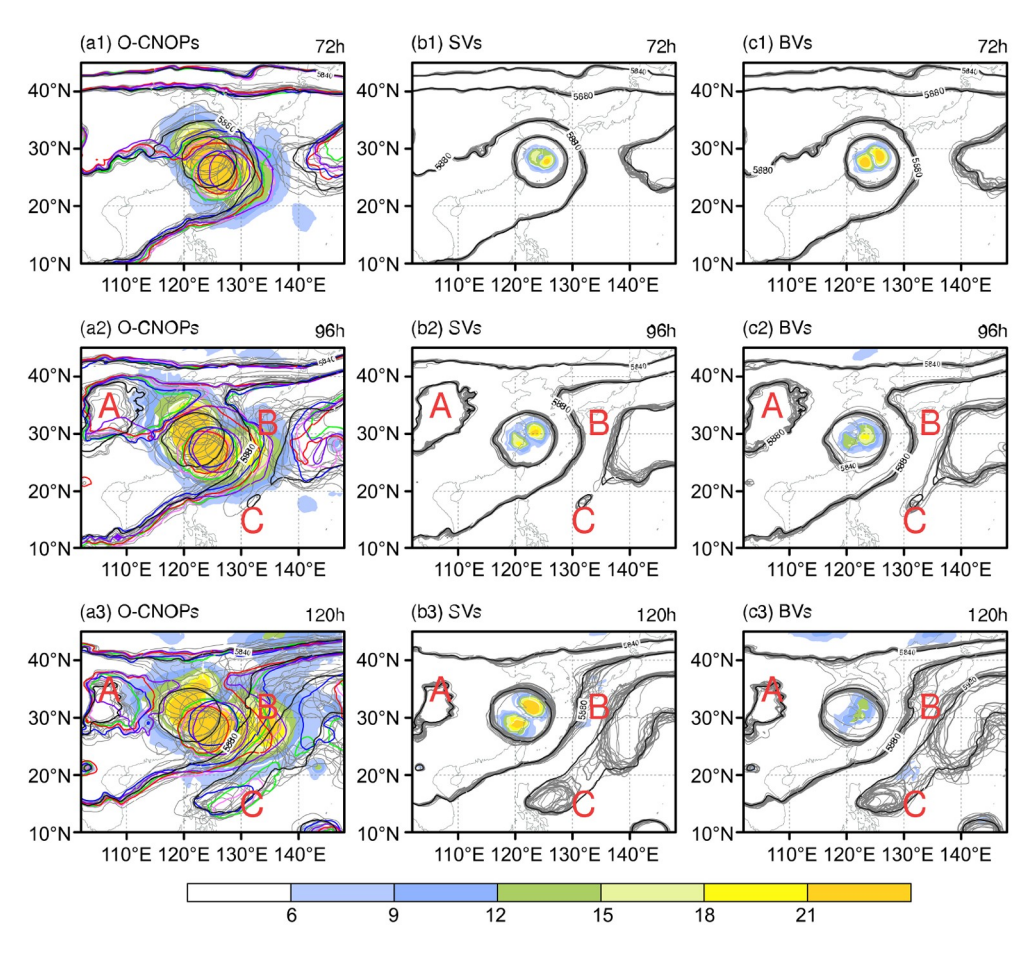


Figure 12 Ensemble spaghetti plots of 500 hPa geopotential height of 5920, 5880 and 5840 gpm (contours), along with their spreads (shaded; unit: gpm), made by the O-CNOPs, SVs, and BVs at lead times of 72 to 120 h for the three ensemble prediction systems. The black contours represent the control forecast, the colored contours represent the five O-CNOPs members that successfully predict the sharp northeastward turn of Khanun (2023), and the gray contours represent the remaining ensemble members.

However, the SVs and BVs ensembles show much less diversity in the intensity and location of the WPSH (see Figure 12b and Figure 12c), leading to a smaller spread in the steering flows surrounding the TC (see Figure 11b and Figure 11c). Therefore, the tracks of Khanun (2023) in both SVs and BVs ensembles exhibit smaller spreads around the control forecast, failing to cover the actual turning location and angle (see Figure 2). As discussed in Section 3.2, both SVs and BVs erroneously predict Khanun (2023) to make landfall on China's eastern coast before turning eastward with a much smaller angle compared to the best track. Conversely, the O-CNOPs ensemble adequately represents the uncertainty associated with the TC's sharp turn, providing a high probability of capturing the northeastward turn of Khanun (2023).

Let us now elucidate the dynamics through which O-CNOPs yield large ensemble spreads in terms of turning location and angle. Initially, Khanun (2023) is steered northwestward by the strong WPSH. At a lead time of about 48 h, the northern WPSH rapidly weakens and eventually splits into two ridges by around 96 h: a weak subtropical

ridge to the west of TC (marked by A in Figure 12) and a subtropical ridge (the main body of the WPSH) to the east of TC (marked by B in Figure 12). The western ridge provides a southward steering flow that counteracts the northward steering flow from the eastern ridge (see Figure 11), causing the TC to slow down before its turn. During this stage, the O-CNOPs ensemble shows large spreads north of Khanun (2023), indicating the uncertainties in the intensity of the WPSH and the location of the eastern and western ridges (see Figure 12a2). These uncertainties may adequately interpret the probability for the strength of the northwestward steering flow and then the northwestward speed of TC movement. Furthermore, the movement speed before the TC turn may affect the farthest northwestward location that TC can reach, i.e., the turning location of Khanun (2023). In the control forecast, the TC track has a much higher northwestward speed than the best track, resulting in a northwestwardbiased turning location relative to the observed turning location. This bias can partly be attributed to the rapid weakening and westward withdrawal of the western ridge in the control forecast, as depicted by the black contours in Figure

12. In contrast, the O-CNOPs ensemble, as shown above, presents a large spread in the TC movement speeds, thereby yielding a large spread in the turning location of Khanun (2023). Some ensemble members, particularly those with a stronger western ridge (represented by the colored contours in Figure 12a), accurately predict the actual turning location. Additionally, as an anticyclone develops on the southern side of TC (marked by C in Figure 12), the southwesterly flow in its northwestern portion strengthens and combines with the southerly flow in the western portion of the eastern ridge (see Figure 11). This interaction forces Khanun (2023) to turn sharply northeastward at a lead time of about 120 h. At this time, the O-CNOPs ensemble shows greater diversity in the intensity and location of the southern and eastern anticyclones, as evidenced by the large spread along the south-toeast portion of the TC (see Figure 12a3). This variability contributes to the large spreads in the relative magnitudes of the northern and western components of the steering flow surrounding TC (see Figure 11a5), and results in a broader spread in the TC moving direction after deflection as well as the turning angle of Khanun (2023). In the control forecast, the TC moves northward rather than northeastward as the best track at lead times of 120 to 144 h. This discrepancy is possibly due to an overestimation of the northward steering flow from an excessively strong eastern ridge and an underestimate of the northeastward steering flow from a relatively weak southern anticyclone. However, these O-CNOPs members with colored contours in Figure 12a, characterized by a stronger southern anticyclone and a much weaker eastern ridge than the control forecast, correct the turning angle of the control forecast, and then make the TC move northeastward after the turn.

In conclusion, the O-CNOPs can provide ensemble members that effectively represent the uncertainties in the surrounding steering flows that influence the TC turn through the dynamic interactions between the TC and the WPSH. This enables O-CNOPs to capture the sharp northeastward turn of Khanun (2023), while both SVs and BVs fail to do so.

4. Summary and discussion

The forecast of unusual TC track remains a challenge in operational forecasting. In this study, we examine the performance of O-CNOPs in improving ensemble forecasting skill for unusual TC tracks. Using the WRF model, we apply O-CNOPs, SVs and BVs to generate initial perturbations and conduct ensemble forecast experiments for the unusual tracks of five TC cases (i.e., Megi (2010), Tembin (2012), Hinnamnor (2022), Khanun (2023) and Saola (2023)), covering twenty-three forecast periods during which the TCs experienced sharp turns. Utilizing these forecasts, we first

evaluate the probabilities of the ensemble members generated by O-CNOPs, BVs and SVs in capturing the sharp turns of TCs. The results reveal that O-CNOPs have a greater capacity to generate more ensemble members that reproduce the sharp turns of TCs at much longer lead times, thereby providing more valuable early warning information on the sharp turns of TC tracks. Furthermore, the ensemble mean forecasts generated by O-CNOPs demonstrate more stable improvements over the control forecasts in predicting TC turns. Results show that O-CNOPs outperform SVs and BVs in predicting the sharp turns of TCs, both in deterministic and probabilistic aspects.

Using Khanun (2023) as an example, this study explains why O-CNOPs outperform SVs and BVs in generating ensemble members that reproduce the sharp TC track turning. That is because O-CNOPs properly identify the energy-related sensitivity of TC movement in the middle to lower troposphere and the dynamics-related sensitivity in the annulus around Khanun (2023). The most unstable structures of O-CNOPs provide ensemble members that effectively depict the large uncertainties in the surrounding steering flow associated with the northeastward turn of Khanun (2023) through the dynamical interaction between Khanun (2023) and the WPSH, thereby capturing the location and angle of the sharp northeastward turn of TC. In contrast, both SVs and BVs fail to do so and miss its sharp northeastward turn. Moreover, the ensemble forecasts generated by O-CNOPs also provide a unique dataset for understanding the dynamical processes that may cause unusual TC movements and limit TC track predictability, offering a possible direction for reducing error sources through targeted observations or model improvements.

The results underscore the great potential of O-CNOPs in enhancing the forecasting reliability of unusual TC tracks. However, it is worth noting that the model resolution adopted in this study (30 km) is still too coarse for some TC cases. For example, all the ensemble forecasts generated by O-CNOPs, BVs and SVs have poor performance in forecasting the looping motion of Saola (2023). This limitation could be attributed to the inability of a 30-km resolution to properly resolve the small-scale TC structure and its interaction with the surrounding environment. Consequently, higher-resolution WRF simulations are needed to address such TC cases. One of the challenges in adopting higher resolutions is the significant computational cost associated with traditional optimization algorithms used to calculate O-CNOPs. Fortunately, recent research by Ma et al. (2025) proposed a parallel iterative method to efficiently calculate O-CNOPs. They demonstrated its high efficiency and effectiveness in ensemble forecasts using an idealized model. By applying this efficient algorithm to a higher-resolution WRF, we anticipate achieving skillful ensemble forecasts of TC tracks in real time. It is also hoped that the application of such an

efficient algorithm can be extended to convective-scale ensemble forecasts for TC intensity, TC-induced precipitation, and other high-impact weather systems.

Nowadays, some data assimilation schemes have been applied to naturally provide initial conditions for ensemble forecasts, such as the Ensemble Kalman Filter (EnKF). These schemes can provide good initial analysis fields and reflect the effect of observational distribution on initial uncertainties (Wang and Bishop, 2003; Ma et al., 2008; Feng et al., 2016). However, they often generate insufficient spread, leading to an underestimation of forecast uncertainties, which commonly requires an inflation coefficient to partially compensate for this limitation (Yang et al., 2015; Zheng and Zhu, 2016; Duan et al., 2019; Li and Zhao, 2022). This study only compares the O-CNOPs method with these traditional initial perturbation methods based on dynamical error growth theory (i.e., BVs and SVs). Future work will compare the performance of O-CNOPs and EnKF for ensemble forecasts of TC tracks. Besides initial errors, model errors also influence TC forecasts. The O-CNOPs method only considers the effect of initial uncertainties to generate ensemble forecasts. Although O-CNOPs achieve better reliability compared to traditional initial perturbation methods, the spread-skill relationship is still imperfect for measuring the reliability of the ensembles. For example, under the configuration determined by Zhang et al. (2023), O-CNOPs tend to overestimate the forecasting uncertainties of TC tracks. Duan et al. (2022) demonstrated that dynamically coordinated growth of initial and model perturbations helps produce ensembles with higher reliability when both initial and model errors are present in forecasts. Therefore, adopting combined modes of initial and model perturbations, such as the C-NFSVs proposed by Duan et al. (2022), is crucial for accounting for the combined effects of initial and model uncertainties in ensemble forecasts and thereby enhancing forecast reliability.

Acknowledgements The authors appreciate the two anonymous reviewers for their insightful comments and suggestions. This work was jointly supported by the National Natural Science Foundation of China (Grant Nos. 41930971) and the International Partnership Program of the Chinese Academy of Sciences (Grant Nos. 060GJHZ2022061MI). The numerical experiments was supported by the National Key Scientific and Technological Infrastructure project "Earth System Numerical Simulation Facility" (EarthLab).

Conflict of interest The authors declare no conflict of interest.

References

- Birgin E G, Martínez J M, Raydan M. 2000. Nonmonotone spectral projected gradient methods on convex sets. SIAM J Optim, 10: 1196–1211
 Chan J C L, Li K K. 2005. Ensemble forecasting of tropical cyclone motion using a barotropic model. Part III: Combining perturbations of the environment and the vortex. Meteorol Atmos Phys, 90: 109–126
- Chen R, Zhang W, Wang X. 2020. Machine learning in tropical cyclone

- forecast modeling: A review. Atmosphere, 11: 676
- Chen Y H, Sha S H, Lin C H, Hsiao L F, Huang C Y, Kuo H C. 2024.
 Performance evaluation of TGFS typhoon track forecasts over the western North Pacific with sensitivity tests on cumulus parameterization. Atmosphere, 15: 1075
- Cheung K K W. 2001. A review of ensemble forecasting techniques with a focus on tropical cyclone forecasting. Meteorol Appl, 8: 315–332
- Cheung K K W, Chan J C L. 1999. Ensemble forecasting of tropical cyclone motion using a barotropic model. Part I: Perturbations of the environment. Mon Weather Rev, 127: 1229–1243
- Conroy A, Titley H, Rivett R, Feng X, Methven J, Hodges K, Brammer A, Burton A, Chakraborty P, Chen G, Cowan L, Dunion J, Sarkar A. 2023.
 Track forecast: Operational capability and new techniques-summary from the tenth international workshop on tropical cyclones (IWTC-10).
 Tropical Cyclone Res Rev, 12: 64–80
- Dai G J, Wen Y R, Li Y. 2014. Statistical characteristics of tropical cyclone motion and sharp turning over northwestern Pacific (in Chinese). J Trop Meteorol, 30: 23–33
- Diaconescu E P, Laprise R. 2012. Singular vectors in atmospheric sciences: A review. Earth-Sci Rev, 113: 161–175
- Duan W S, Huo Z H. 2016. An approach to generating mutually independent initial perturbations for ensemble forecasts: Orthogonal conditional nonlinear optimal perturbations. J Atmos Sci, 73: 997–1014
- Duan W S, Li X Q, Tian B. 2018. Towards optimal observational array for dealing with challenges of El Niño-Southern Oscillation predictions due to diversities of El Niño. Clim Dyn, 51: 3351–3368
- Duan W S, Ma J J, Vannitsem S. 2022. An ensemble forecasting method for dealing with the combined effects of the initial and model errors and a potential deep learning implementation. Mon Weather Rev, 150: 2959– 2976
- Duan W S, Wang Y, Huo Z H, Zhou F F. 2019. Ensemble forecast methods for numerical weather forecast and climate prediction: Thinking and prospect (in Chinese). Clim Environ Res, 24: 396–406
- Dube A, Ashrit R, Kumar S, Mamgain A. 2020. Improvements in tropical cyclone forecasting through ensemble prediction system at NCMRWF in India. Tropical Cyclone Res Rev. 9: 106–116
- Feng J, Ding R Q, Li J P, Liu D Q. 2016. Comparison of nonlinear local Lyapunov vectors with bred vectors, random perturbations and ensemble transform Kalman filter strategies in a barotropic model. Adv Atmos Sci, 33: 1036–1046
- Gong Y, Li Y, Zhang D L. 2018. A statistical study of unusual tracks of tropical cyclones near Taiwan Island. J Appl Meteorol Climatol, 57: 193–206
- Huo Z H, Duan W S, Zhou F F. 2019. Ensemble forecasts of tropical cyclone track with orthogonal conditional nonlinear optimal perturbations. Adv Atmos Sci, 36: 231–247
- Lang S T K, Leutbecher M, Jones S C. 2012. Impact of perturbation methods in the ECMWF ensemble prediction system on tropical cyclone forecasts. Q J R Meteorol Soc, 138: 2030–2046
- Lei L, Ge Y, Tan Z M, Zhang Y, Chu K, Qiu X, Qian Q. 2022. Evaluation of a regional ensemble data assimilation system for typhoon prediction. Adv Atmos Sci, 39: 1816–1832
- Li Y, Heming J, Torn R D, Lai S, Xu Y, Chen X. 2023. Unusual tracks: Statistical, controlling factors and model prediction. Tropical Cyclone Res Rev, 12: 309–322
- Li Y, Zhao D. 2022. Climatology of tropical cyclone extreme rainfall over China from 1960 to 2019. Adv Atmos Sci, 39: 320–332
- Liu L, Feng J, Ma L, Yang Y, Wu X, Wang C. 2024. Ensemble-based sensitivity analysis of track forecasts of typhoon In-fa (2021) without and with model errors in the ECMWF, NCEP, and CMA ensemble prediction systems. Atmos Res, 309: 107596
- Lorenz E N. 1996. Predictability: A problem partly solved. Workshop on Predictability, Reading, United Kingdom, ECMWF, 1: 1–18
- Ma J J, Duan W S, Liu Z M, Wang Y. 2025. A new method to calculate nonlinear optimal perturbations for ensemble forecasting. Adv Atmos Sci, 42: 952–967
- Ma M, Peng M S, Li T, Wang L. 2022. Understanding the unusual track of

- Typhoon Lionrock (2016). Weather Forecast, 37: 393-414
- Ma X L, Xue J S, Lu W S. 2008. Preliminary study on ensemble transform Kalman filter-based initial perturbation scheme in GRAPES global ensemble prediction (in Chinese). Acta Meteorol Sin, 4: 526–536
- Magnusson L, Doyle J D, Komaromi W A, Torn R D, Tang C K, Chan J C L, Yamaguchi M, Zhang F. 2019. Advances in understanding difficult cases of tropical cyclone track forecasts. Tropical Cyclone Res Rev, 8: 109–122
- Miller W, Zhang D L. 2019. Understanding the unusual looping track of hurricane joaquin (2015) and its forecast errors. Mon Weather Rev, 147: 2231–2259
- Miyachi T, Enomoto T. 2021. Tropical cyclone track forecasts using NCEP-GFS with initial conditions from three analyses. SOLA, 17: 140–144
- Nie G Z, Xu Y L, Wang H P. 2025. Analysis of the characteristics and forecast difficulties of typhoon activities in the western North Pacific in 2023 (in Chinese). Meteorol Mon, 51: 369–381
- Palmer T. 2019. The ECMWF ensemble prediction system: Looking back (more than) 25 years and projecting forward 25 years. Q J R Meteorol Soc. 145: 12–24
- Pattanayak S, Mohanty U C. 2008. A comparative study on performance of MM5 and WRF models in simulation of tropical cyclones over Indian seas. Curr Sci, 95: 923–936
- Puri K, Barkmeijer J, Palmer T N. 2001. Ensemble prediction of tropical cyclones using targeted diabatic singular vectors. Q J R Meteorol Soc, 127: 709-731
- Qian Q F, Mao D Y. 2023. Evaluation of tropical cyclone track forecast performance of ECMWF and NCEP ensemble models from 2010 to 2019 (in Chinese). Meteorol Mon, 49: 224–234
- Qian W, Du J, Ai Y, Leung J, Liu Y, Xu J. 2024. Anomaly-based variable models: Examples of unusual track and extreme precipitation of tropical cyclones. Meteorology, 3: 243–261
- Skamarock W, Klemp J, Dudhia J, Gill D O, Barker D, Duda M G, Huang X Y, Huang W, Powers J G. 2008. A description of the advanced research WRF version 3. NCAR Technical Note, NCAR/TN-475+STR
- Tang C K, Chan J C L, Yamaguchi M. 2021. Large tropical cyclone track forecast errors of global numerical weather prediction models in western North Pacific basin. Tropical Cyclone Res Rev, 10: 151–169
- Thanh C, Tien T T, Chanh K Q. 2016. Application of breeding ensemble to

- tropical cyclone track forecasts using the Regional Atmospheric Modeling System (RAMS) model. Appl Math Model, 40: 8309–8325
- Torn R D, Elless T J, Papin P P, Davis C A. 2018. Tropical cyclone track sensitivity in deformation steering flow. Mon Weather Rev, 146: 3183– 3201
- Toth Z, Kalnay E. 1993. Ensemble forecasting at NMC: The generation of perturbations. Bull Amer Meteorol Soc, 74: 2317–2330
- Toth Z, Kalnay E. 1997. Ensemble forecasting at NCEP and the breeding method. Mon Weather Rev, 125: 3297–3319
- Tseng J C H, Lai Y S. 2020. Perturbation structure and evolution in tropical cyclones Noul and Nepartak based on singular vectors. Tellus A-Dynamic Meteorol Oceanogr, 72: 1814589
- Wang C X, Ni Y Q. 2011. Sensitivity experiments of impacting tropical cyclone track (in Chinese). Acta Meteorol Sin, 69: 757–769
- Wang X, Bishop C H. 2003. A comparison of breeding and ensemble transform Kalman filter ensemble forecast schemes. J Atmos Sci, 60: 1140–1158
- Xiang C, Ying L X, Shuan Z G, Qian W, Haiping W. 2022. Analysis of the characteristics and forecast difficulties of typhoon over the western North Pacific in 2021 (in Chinese). Meteorol Mon, 48: 1195–1208
- Yamaguchi M, Majumdar S J. 2010. Using TIGGE data to diagnose initial perturbations and their growth for tropical cyclone ensemble forecasts. Mon Weather Rev, 138: 3634–3655
- Yamaguchi M, Sakai R, Kyoda M, Komori T, Kadowaki T. 2009. Typhoon ensemble prediction system developed at the Japan Meteorological Agency. Mon Weather Rev, 137: 2592–2604
- Yang S C, Kalnay E, Enomoto T. 2015. Ensemble singular vectors and their use as additive inflation in EnKF. Tellus A-Dynamic Meteorol Oceanogr, 67: 26536
- Zhang X, Li Y, Zhang D L, Chen L. 2018. A 65-yr climatology of unusual tracks of tropical cyclones in the vicinity of China's coastal waters during 1949–2013. J Appl Meteorol Climatol, 57: 155–170
- Zhang H, Duan W S, Zhang Y C. 2023. Using the orthogonal conditional nonlinear optimal perturbations approach to address the uncertainties of tropical cyclone track forecasts generated by the WRF model. Weather Forecast, 38: 1907–1933
- Zheng F, Zhu J. 2016. Improved ensemble-mean forecasting of ENSO events by a zero-mean stochastic error model of an intermediate coupled model. Clim Dyn, 47: 3901–3915

(Editorial handling: Lili LEI)



论 文



用O-CNOPs方法改进异常台风路径集合预报的可靠性

张晗^{1,2,6}, 段晚锁^{2*}, 黄永杰³, 陈柏纬⁴, Stephane VANNITSEM⁵

- 1. 中国气象局河南省农业气象保障与应用技术重点开放实验室、郑州 450003
- 2. 中国科学院大气物理研究所大气科学和地球流体力学数值模拟国家重点实验室, 北京 100029
- 3. Center for Analysis and Prediction of Storms and School of Meteorology University of Oklahoma, Norman Oklahoma 73072, USA
- 4. 香港天文台, 香港 999077
- 5. Royal Meteorological Institute of Belgium, Brussels 1180, Belgium
- 6. 河南省气象台, 郑州 450003
- * 通讯作者, E-mail: duanws@lasg.iap.ac.cn

收稿日期: 2025-04-09; 收修改稿日期: 2025-08-04; 接受日期: 2025-08-19; 网络版发表日期: 2025-10-16 国家自然科学基金项目(41930971)和中国科学院国际伙伴计划项目(060GJHZ2022061MI)资助

摘要 异常台风路径预报面临巨大挑战. 本文将正交条件非线性最优扰动(O-CNOPs)方法应用于WRF模式, 选取5个具有异常路径特征的台风个例(含23个对台风转向预报的时段), 系统对比了O-CNOPs、奇异向量(SVs)和繁殖向量(BVs)三类扰动方法集合预报性能的可靠性. 结果表明, 无论是确定性预报还是概率预报, O-CNOPs方法均较SVs和BVs能够更稳定、更可靠地提升台风路径预报技巧, 尤其O-CNOPs在提前1~5天预报台风路径时, 能够更早且有更高概率地准确预报台风路径的异常转向. 所以, 与传统的SVs和BVs方法相比, O-CNOPs在提升台风路径预报技巧, 尤其是异常路径的预报技巧方面, 具有明显优势, 希望O-CNOPs在未来提升台风业务预报水平中发挥重要作用.

关键词 台风,集合预报,最优扰动

1 引言

西北太平洋台风常给中国带来极端大风和暴雨等灾害,严重威胁人民的生命财产安全(Li和Zhao, 2022). 台风风雨的预报精度在很大程度上依赖于台风路径预报准确率(Conroy等, 2023; Qian等, 2024). 因此,精准的台风路径预报对于减轻台风灾害影响至关重要. 近几十年来,台风路径预报水平取得了长足进步,但长时效路径预报与异常路径预报依然面临诸多挑战.异常路径的长时效预报尤为困难(Zhang等,2018; Chen等,2020; Tang等,2021; Li等,2023; Liu等,2024). 近年来,异常台风路径在西北太平洋频发,给业务预报造成了巨大挑战.例如,2021年台风"烟花"路径在西行过程中突然发生北折,而大多数预报中心未

中文引用格式: 张晗, 段晚锁, 黄永杰, 陈柏纬, Vannitsem S. 2025. 用O-CNOPs方法改进异常台风路径集合预报的可靠性. 中国科学: 地球科学, 55, doi:

10.1360/N072025-0124

英文引用格式: Zhang H, Duan W, Huang Y, Chan P W, Vannitsem S. 2025. Improve the forecast reliability of unusual tropical cyclone tracks using ensemble forecasts generated by O-CNOPs. Science China Earth Sciences, https://doi.org/10.1007/s11430-025-1668-1

© 2025 《中国科学》杂志社 www.scichina.com

能提前3天准确预报这一转向过程,即使在临近其转向时开始预报,部分预报中心也仍难以再现"烟花"的北折路径,其路径预报误差远高于2021年平均路径预报误差(向纯怡等,2022; Li等,2023; Liu等,2024). 类似地,2023年台风"卡努"生成初期,欧洲中期天气预报中心(ECMWF)和美国国家环境预报中心(NCEP)等主流预报中心均预测其将登陆中国,但"卡努"在行进过程中突然转向东北移动,完全避开了中国(聂高臻等,2025);随后,尽管预报显示其可能袭击日本,但"卡努"再次出现向北急转弯,最终登陆韩国.同年,各家业务预报中心未能准确预报台风"苏拉"生成初期的打转过程,导致登陆点预报误差偏大.由此可见,长时效路径预报通常难以再现异常台风路径;即使在台风临近转向时起报,路径预报仍存在着较大的不确定性.

目前,集合预报被广泛应用于业务部门,是提高台 风预报技巧、估计预报不确定性并提供概率预报的重 要手段(Puri等, 2001; Dube等, 2020). 集合预报方法的 发展极大推动了台风预报水平的提升(Duan等, 2018; Zhang等, 2023). 台风路径主要受环境引导气流控制, 对初始场的变化高度敏感(Yamaguchi和Majumdar, 2010; 王晨稀和倪允琪, 2011; Miller和Zhang, 2019; Miyachi和Enomoto, 2021; Ma等, 2022; Zhang等, 2023), 这种敏感性凸显了初始不确定性在台风路径预 报中的重要作用. 研究表明, 在控制预报上叠加快速增 长型初始扰动来描述初始不确定性、是改进集合预报 可靠性的关键(Toth和Kalnay, 1993, 1997; Palmer, 2019; Magnusson等, 2019). ECMWF采用奇异向量 (SVs)方法, 而NCEP曾使用繁殖向量(BVs)方法来刻画 初始不确定性, SVs和BVs均旨在产生快速增长型初始 扰动, 以反映预报误差的增长特性, 从而充分表征预报 不确定性, 在台风路径集合预报中取得了巨大成功 (Cheung和Chan, 1999; Cheung, 2001; Yamaguchi等, 2009; Yamaguchi和Majumdar, 2010; Diaconescu和Laprise, 2012; Magnusson等, 2019; Palmer, 2019). 然而, 这两类扰动方法也存在一些局限性. BVs刻画了预报 时段之前快速增长的扰动, 难以在长预报时效维持增 长, 常导致集合离散度偏小, 使实况路径落在预报集 合之外(Chan和Li, 2005; Lang等, 2012; Thanh等, 2016; Zhang等, 2023). SVs是线性模式中增长最快的 初始扰动,不能充分刻画大气运动中非线性物理过程 的影响, 因而可能会低估预报不确定性(Puri等, 2001; Lang等, 2012; Huo等, 2019; Zhang等, 2023).

为了全面考虑非线性物理过程的影响, Duan和 Huo(2016)将SVs拓展到非线性领域、提出了正交条件 非线性最优扰动(O-CNOPs)方法. O-CNOPs代表了在 一定时段内, 不同相空间中具有最大非线性发展的一 组正交初始扰动(Duan和Huo, 2016; Huo等, 2019; Zhang等, 2023). Duan和Huo(2016)利用简单的Lorenz-96模式验证了O-CNOPs的动力学合理性、发现其集合 预报技巧高于SVs方法. 进一步地, Huo等(2019)将O-CNOPs方法应用于MM5模式进行台风路径集合预报. 其表现优于传统的随机扰动(RPs)、BVs和SVs方法. WRF模式比MM5模式更为先进,对台风路径的模拟能 力更强(Pattanayak和Mohanty, 2008). 后续研究基于 WRF模式进一步验证了O-CNOPs方法的优越性. Zhang等(2023)将O-CNOPs方法应用于WRF模式开展 台风路径集合预报试验, 其确定性和概率预报技巧均 高于BVs和SVs方法. 因此, O-CNOPs方法在提高台风 路径预报水平方面具有重要潜力、在业务预报中具有 广阔的应用前景.

如前所述,异常台风路径的长时效预报十分困难,而目前尚无研究对 O-CNOPs方法在异常路径预报中的表现进行系统性评估. 由此引出一个关键问题: O-CNOPs方法是否能够显著提升异常台风路径的预报技巧? 为了回答这一问题,该研究将O-CNOPs方法应用于WRF模式,针对异常台风路径开展集合预报试验研究.

2 O-CNOPs方法和WRFV3.6模式

将O-CNOPs方法应用于WRFV3.6模式(Skamarock等, 2008)生成集合初始扰动,针对异常台风路径开展集合预报试验. 尽管Zhang等(2023)已将WRFV3.6与O-CNOPs相结合用于台风路径集合预报,但并未聚焦于异常台风路径. 本文沿用WRFV3.6模式,但对O-CNOPs方法的应用策略进行了调整,专门针对异常台风路径开展集合预报试验. 本文不再赘述WRFV3.6模式的具体配置,相关细节可参考 Zhang等(2023). 本节重点介绍O-CNOPs方法的具体应用策略.

O-CNOPs(记为 \mathbf{x}_{0j}^* , j=1, 2, 3,...)是一组相互正交的 初始扰动,它们在给定的优化时段[0, τ](即OTI; 见 Zhang等, 2023)内,在各自对应的子空间(Ω_i)中具有最

大非线性发展(Duan和Huo, 2016). 第j个CNOP是如下优化问题(方程(1))的解:

$$\mathbf{J}(\mathbf{x}_{0j}^{*}) = \max_{\mathbf{x}_{0j} \in \Omega_{j}} \left[PM_{\tau}(\mathbf{X}_{0} + \mathbf{x}_{0j}) - PM_{\tau}(\mathbf{X}_{0}) \right]^{\mathrm{T}} \times \mathbf{C}_{2} \left[PM_{\tau}(\mathbf{X}_{0} + \mathbf{x}_{0j}) - PM_{\tau}(\mathbf{X}_{0}) \right], \tag{1}$$

其中, 子空间 Ω_i 是

$$\Omega_{j} = \left\{ \left\{ \mathbf{x}_{0j} \in \mathbf{R}^{n} \middle| \mathbf{x}_{0j}^{\mathsf{T}} \mathbf{C}_{1} \mathbf{x}_{0j} \leq \delta \right\}, \qquad j = 1, \\ \left\{ \left\{ \mathbf{x}_{0j} \in \mathbf{R}^{n} \middle| \mathbf{x}_{0j}^{\mathsf{T}} \mathbf{C}_{1} \mathbf{x}_{0j} \leq \delta, \mathbf{x}_{0j} \perp \Omega_{k}, k = 1, \dots, j - 1 \right\}, \quad j > 1, \right\}$$

 $X_0 \in R^n$ 表示状态向量, M是数值模式的非线性传播算子. 上标"T"表示转置, δ >0表示最大初始扰动振幅. P是一个局地投影算子,在验证区域(即预报关注区域)内取值为1,区域外取值为0. 本研究将验证区域设定为以优化时刻台风位置为中心的 $10^{\circ} \times 10^{\circ}$ 范围,提取该时刻台风环流相关的不确定性特征(Tseng和Lai,2020),而初始扰动区域则覆盖整个模拟区域. 在方程(1)和(2)中, C_1 和 C_2 均选取为总湿能量(TMEs)作为目标函数,定义如下(方程(3)):

$$\|\delta \mathbf{X}\|_{C_{1}}^{2} = \|\delta \mathbf{X}\|_{C_{2}}^{2}$$

$$= \frac{1}{D} \int_{D} \int_{0}^{1} \left[\mathbf{u}'^{2} + \mathbf{v}'^{2} + \left(\frac{g}{N \theta} \right)^{2} \mathbf{\theta}'^{2} + R_{a} T_{r} \left(\frac{\mathbf{p}'_{s}}{p_{r}} \right)^{2} + \frac{L^{2}}{c_{p} T_{r}} \mathbf{q}'^{2} \right] d\sigma dD,$$
(3)

其中, \mathbf{u}' 、 \mathbf{v}' 、 $\mathbf{\theta}'$ 、 \mathbf{p}'_s 和 \mathbf{q}' 分别表示扰动纬向风、经向风、位温、表层气压和水汽混合比; $\overline{\theta}$ =300K, T_r =270K和 p_r =1000hPa为参考物理参数; g为重力加速度, R_a 和 \mathbf{c}_p 是干空气的气体常数和定压比热容, \overline{N} 是Brunt-Vaisala频率,L是单位质量水汽的凝结潜热。动能项和势能项(\mathbf{u}' 、 \mathbf{v}' 、 $\mathbf{\theta}'$ 和 \mathbf{p}'_s)在垂直方向上进行整层积分,而水汽项(\mathbf{q}')仅从1000hPa至500hPa进行垂直积分。

根据Zhang等(2023)的试验结果, 当OTI = 6h, 初始 扰动振幅 δ =1.8、集合成员数N=21时,O-CNOPs方法 在台风路径集合预报中实现了最高的集合预报技巧. 该研究沿用这一最优集合参数配置.与Zhang等(2023) 一致,该研究仍采用SPG2迭代算法(Birgin等,2000)求 解最优化问题(1),从而获得O-CNOPs型初始扰动.考 虑到异常台风运动受到多尺度相互作用的影响,该研 究在集合预报试验中采用了更高的模式分辨率,即水平分辨率为 30km, 垂直层数为31层(自地面向上延伸至50hPa). 不同的是, Zhang等(2023)在粗分辨率(水平分辨率为60km, 垂直层数为15层)下完成O-CNOPs的求解与集合预报试验;该研究则仅在这一粗分辨率下计算O-CNOPs,随后将其线性插值到更高分辨率(30km水平分辨率,31层垂直层数),作为集合预报试验的初始扰动. 基于10个独立的初始扰动,生成21个集合成员. 具体而言,将初始扰动以正负扰动对的形式叠加在控制预报的初始场,产生20个初始扰动场.利用高分辨率的WRFV3.6模式对这些初始场进行积分,得到 20个扰动预报. 将这些扰动预报与控制预报结合,共同构成21个集合预报成员. 其中,控制预报的初始条件和边界条件由NCEP的全球预报系统(GFS)数据集提供,其水平分辨率为1.0°×1.0°,时间分辨率为6h

为了评估O-CNOPs方法的预报性能,我们将对比O-CNOPs与传统方法(即ECMWF采用的SVs方法和NCEP曾采用的BVs方法)的台风路径集合预报结果.SVs和BVs的集合参数配置也与Zhang等(2023)一致.Zhang等(2023)曾尝试多种集合参数组合,结果均显示SVs和BVs的集合预报技巧普遍低于O-CNOPs.SVs和BVs的简要介绍可参见Zhang等(2023)附录A.

3 异常台风路径的集合预报

本节将选取具有异常路径的台风个例,对比研究 O-CNOPs与SVs、BVs在提高异常台风路径预报技巧 中的作用.

3.1 台风个例

为了针对性地研究异常台风路径的预报技巧,首 先有必要区分异常路径和常规路径.然而,目前尚未 有一个普适的标准来定义异常台风路径(Li等,2023). 在中国的业务预报中,台风移向突变的标准是12h内 右折超过45°或左折超过30°,这一标准被广泛应用到 异常台风路径的相关研究中(Gong等,2018). 戴高菊 等(2014)的统计表明,在西北太平洋上,12h内右折大 于45°的台风路径出现概率小于2.8%,而左折大于30° 的台风路径出现概率小于8.7%.这一研究结果为上述 标准提供了理论依据,意味着采用上述阈值可以有效 地筛选出足够异常的台风路径,将其与缓慢转向路径区分开来.此外,这里不考虑台风路径的短期振荡,要求台风转折后保持相对稳定的移动方向.根据上述标准,从2022年和2023年选取了三个具有异常路径的台风个例——2022年台风"轩岚诺"、2023年台风"卡努"和"苏拉".尽管Zhang等(2023)未聚焦于异常台风路径,但其中的2010年台风"鲇鱼"和2012年台风"天秤"也符合上述标准,因此也被纳为研究对象.以上5个台风个例均对中国产生了显著影响.

图1展示了以上5个台风个例的异常路径,标注了6个异常转向点(图1中红色星号). 其中,"鲇鱼"和"轩岚诺"的路径突然北翘,"卡努"的路径呈现"Z"型特征(分别于2023年8月4日在中国东海洋面上、8月7日在日本南部洋面上发生向东北和向北的两次急转弯),"天秤"和"苏拉"的路径则出现逆时针打转.针对5个台风个例,共选取了18个预报时段(详见表1).由于不同台风个例的生命史不同,预报时长也不尽相同,在5~10天之间.由于"卡努"发生了两次急转向(对应2个异常转

向点),6个异常转向点共涉及了23次集合预报试验,

3.2 台风急转向的集合预报技巧

在6个异常转向点的23次集合预报试验中,每次预报包含21个集合成员,三种方法(O-CNOPs、SVs和BVs)各累计生成483个集合成员.基于所得集合预报结果,本节首先评估了三种方法对台风异常转向预报的概率预报技巧,并通过计算转向阶段的路径误差,进一步评估其集合平均预报性能.

图2、图3、图4给出了控制预报以及O-CNOPs、SVs和BVs生成的台风路径集合预报结果. 由图可见,控制预报难以准确把握台风异常转向的时间、位置和角度,尤其是在台风急转向前较早时段起报时,其移动路径极大地偏离最佳路径. 在这种情况下,合理的集合预报需要充分表征预报不确定性, 使集合成员尽可能覆盖最佳路径. 但如图所示, BVs和SVs生成的集合成员大多紧密围绕在控制预报附近, 尤其是在长时效预报中,使最佳路径落在预报集合之外. 与之不同, O-

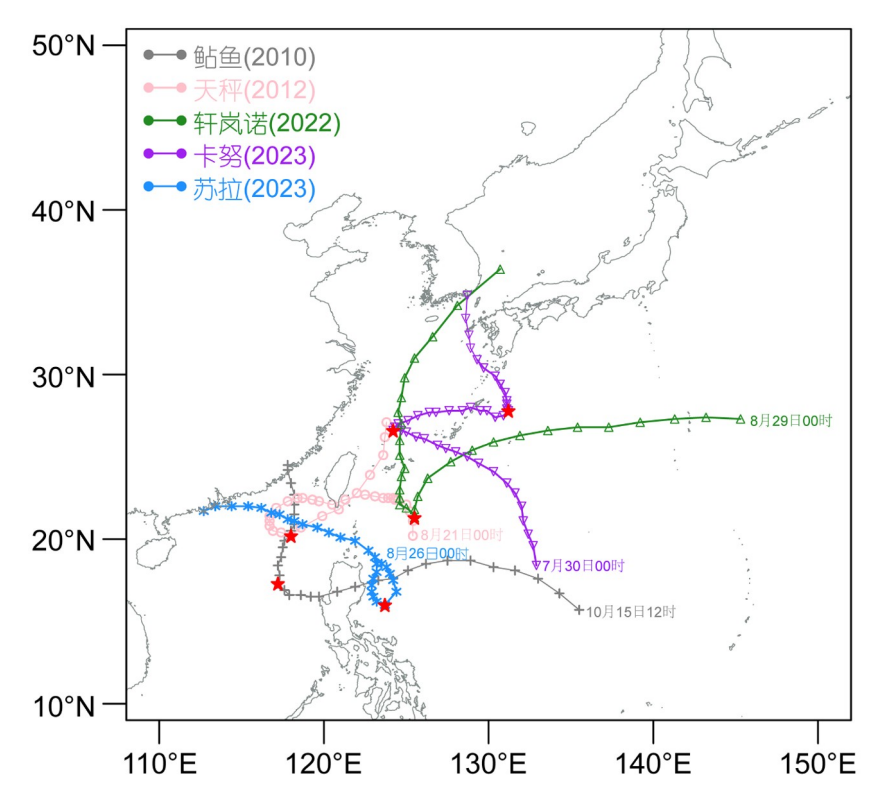


图 1 本文选取的5个台风个例在预报时段内的实况路径

数据来自于中国气象局(CMA)热带气旋最佳路径数据集. 图中每个台风路径的起点是这些台风个例在第一个起报时刻(见表1)的台风位置, 随后每6h一个标记点, 红色星号标注台风路径的异常转向点

台风个例	预报时段(协调世界时)	O-CN	NOPs	SV	⁷ S	BA	/s
	2010年10月15日12:00至2010年10月23日12:00	1	/	×		×	
鲇鱼	2010年10月16日12:00至2010年10月23日12:00	\checkmark		×		×	
	2010年10月17日12:00至2010年10月23日12:00	\checkmark		×			
	2010年10月18日12:00至2010年10月23日12:00	١	/	\checkmark		$\sqrt{}$	
天秤	2012年8月21日00:00至2012年8月29日00:00	١	/	×		×	
	2012年8月22日00:00至2012年8月29日00:00	>	<	×		×	
	2012年8月23日00:00至2012年8月29日00:00	١	/	\checkmark		$\sqrt{}$	
轩岚诺	2022年8月29日00:00至2022年9月6日00:00	>	<	×		×	
	2022年8月30日00:00至2022年9月6日00:00	√ ×		×			
	2022年8月31日00:00至2022年9月6日00:00	$\sqrt{}$		$\sqrt{}$			
	2022年9月1日00:00至2022年9月6日00:00	√ ×		:	×		
卡努	2023年7月30日00:00至2023年8月9日00:00	$\sqrt{}$	×	×	×	×	×
	2023年7月31日00:00至2023年8月10日00:00	$\sqrt{}$	$\sqrt{}$	×	×	×	×
	2023年8月1日00:00至2023年8月10日00:00	$\sqrt{}$	×	×	×	×	×
	2023年8月2日00:00至2023年8月10日00:00	$\sqrt{}$	$\sqrt{}$	×	×	×	×
	2023年8月3日00:00至2023年8月10日00:00	$\sqrt{}$	$\sqrt{}$	$\sqrt{}$	×	$\sqrt{}$	×
苏拉	2023年8月26日00:00至2023年9月2日00:00	×		×		×	
	2023年8月27日00:00至2023年9月2日00:00	$\sqrt{}$		×		×	

表 1 5个台风个例选取的预报时段(协调世界时, 下同)^{a)}

CNOPs生成的集合成员展现出更大的离散度,更多成员显著偏离控制预报并更有可能覆盖最佳路径. 统计表明,在23次预报中,实际转向点、转向时间和转向角度同时落在O-CNOPs集合成员组成的预报范围内的次数达18次,而SVs和BVs对应的次数分别为5次和4次. 因此,与SVs和BVs方法相比,O-CNOPs集合预报更有可能捕捉到台风异常转向.

为了进一步量化O-CNOPs方法成功捕捉台风异常转向(包括转向位置、时间和角度)的概率,该研究引入"可接受误差范围"概念,分别为转向位置、时间和角度设定可接受误差上限(见表2). 鉴于目前尚无衡量台风转向预报成功与否的指标,我们设计了这种非常规评估方法. 在实际业务预报中,此类概率评估可为决策者提供有价值的预警信息. 通过对表2设定的可接受误差上限进行组合,构建27种不同精度等级的评估方案. 图5给出了在23次试验的483个集合成员中,不同精度等级下成功预报台风异常转向的集合成员占比. 结果表明,无论采用何种精度等级,O-CNOPs集合

预报中成功集合成员占比(10%~63%)均持续且显著地高于SVs(3%~38%)及BVs(2%~33%). 换言之, O-CNOPs方法能够产生更多的集合成员来再现台风异常转向, 更可靠地估计台风急转向的发生概率, 从而为台风路径预报和防灾减灾决策提供更有力的支持.

以转向位置、转向时间和转向角度的可接受误差上限为120km、12h和10°为例,图6更详细地统计了在24、48、72、96和120h预报时效下,成功预报出台风异常转向的集合成员占比.注意到,在5个台风个例中,控制预报仅能在1~2天预报时效内将转向时间和转向位置误差控制在上述120km、12h的误差范围内,但仍未能准确预报转向角度(见图4).由图6可见,在转向前1~5天起报时,O-CNOPs方法均能够生成更多的集合成员再现台风急转向.具体地,超过50%的O-CNOPs集合成员能够提前1~3天成功捕捉台风急转向;在4天预报时效下,成功率仍接近50%;即使在转向前5天起报,仍有超过30%的O-CNOPs集合成员成功捕捉到台风急转向.然而,SVs和BVs方法仅在1~2天预报时效

a) 对号($\sqrt{}$)表示O-CNOPs、SVs或BVs的集合成员成功覆盖了最佳路径的转向位置、转向时间和转向角度. 错号(\times)则表示集合成员未能覆盖这些关键的转向特征

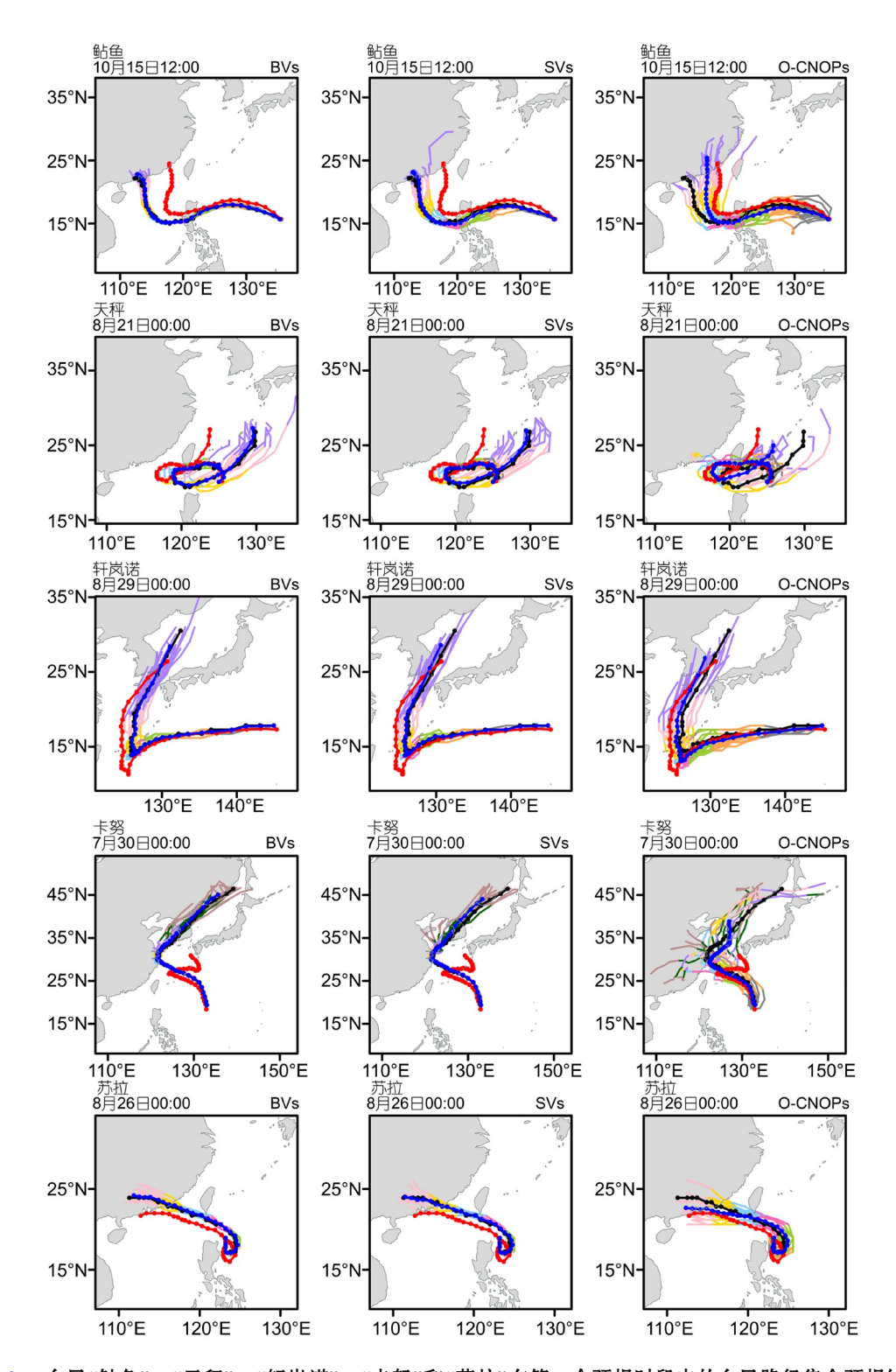


图 2 台风"鲇鱼"、"天秤"、"轩岚诺"、"卡努"和"苏拉"在第一个预报时段内的台风路径集合预报结果 从左到右分别表示BVs、SVs和O-CNOPs方法;图中红色、黑色和蓝色点线分别是最佳路径,控制预报和集合平均路径预报,每6h一个标记

从左到右分别表示BVs、SVs和O-CNOPs方法;图中红色、黑色和蓝色点线分别是最佳路径,控制预报和集合平均路径预报,每6h一个标记点.不同预报时段内的扰动成员路径由不同颜色表示:0~24h(灰色)、24~48h(橙色)、48~72h(浅绿色)、72~96h(品红色)、96~120h(浅蓝色)、120~144h(黄色)、144~168h(粉红色)、168~192h(紫色)、192~216h(深绿色)和216~240h(褐色)

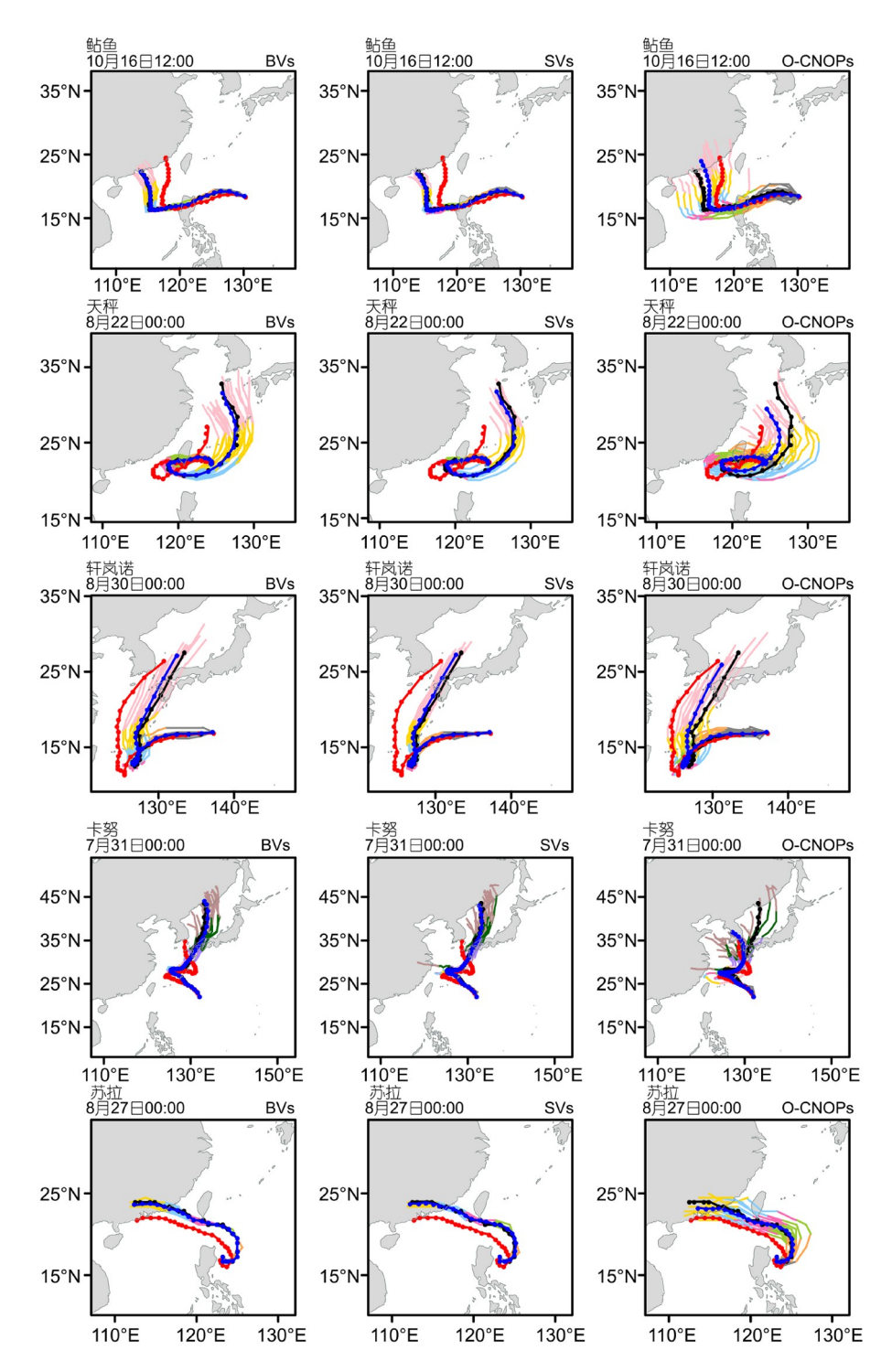


图 3 同图2, 但为台风"鲇鱼"、"天秤"、"轩岚诺"、"卡努"和"苏拉"在第二个预报时段内的台风路径集合预报结果

内有超过50%的成功率;超过3天预报时效后,其成功率急剧下降;在4~5天预报时效下,成功率不足10%,严重限制了它们对台风路径突变的提前预警能力.例如,

在台风"卡努"首次急转弯前5天起报时,控制预报及 SVs、BVs生成的集合成员均错误地预报其将登陆中 国东南沿海;而约30%的O-CNOPs集合成员已预报出

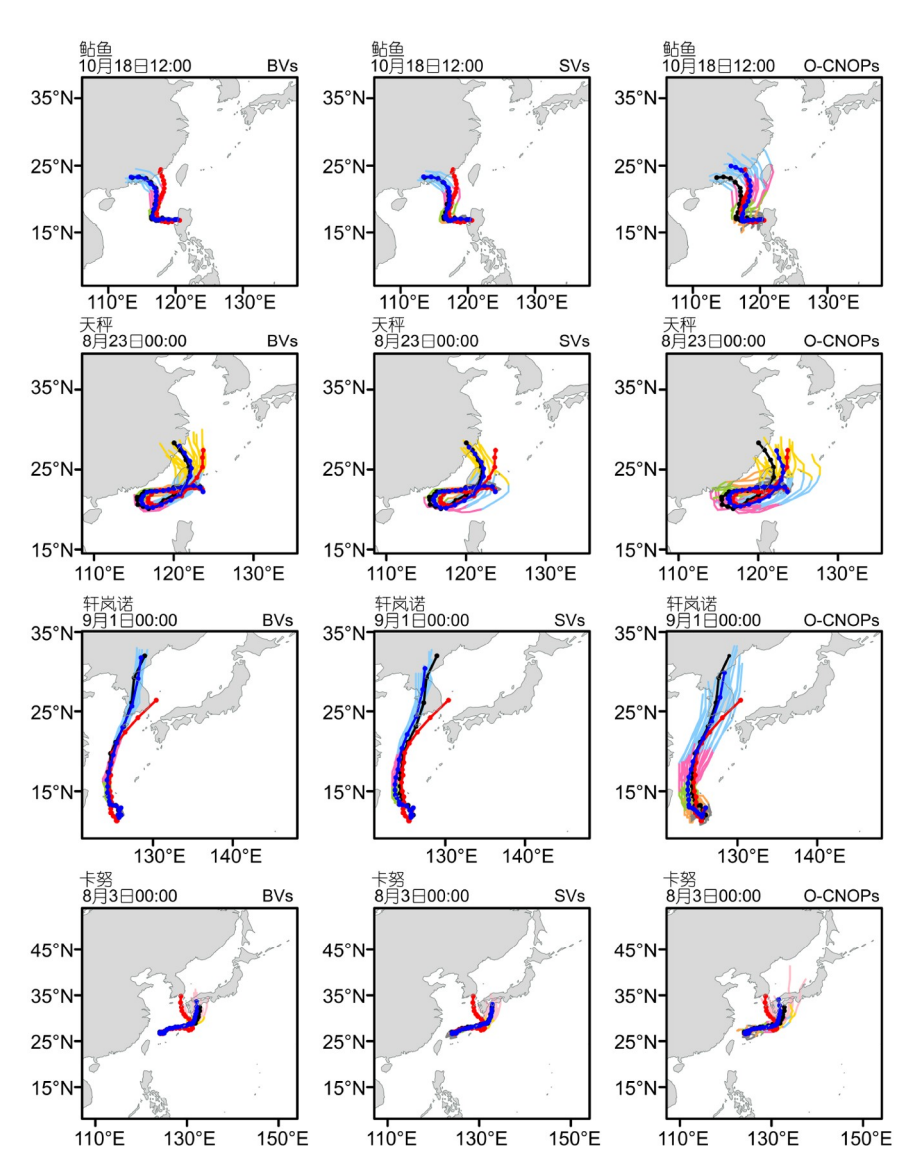


图 4 同图2, 但为台风"鲇鱼"、"天秤"、"轩岚诺"、"卡努"和"苏拉"在最后一个预报时段内的台风路径集合预报结果

表 2 判定台风异常转向预报(包括转向位置、时间和角度) 是否准确的可接受误差上限

预报误差上限	转向位置	转向时间	转向角度		
1	60km	6h	5°		
2	120km	12h	10°		
3	180km	18h	15°		

其向东北方向的急转弯(见图2). 由此可见, O-CNOPs 方法能够在更长的预报时效内生成更多成功捕捉台风 急转向的集合成员, 有利于提高台风路径突变的预警能力.

进一步地,定量分析SVs、BVs和O-CNOPs生成的集合平均预报对台风异常转向的预报能力.首先,比较控制预报与三类集合平均预报的转向位置误差和转向时间误差.如图7所示,O-CNOPs集合平均预报的转向位置误差和转向时间误差(152km、8h)明显小于控制预报(225km、11h).尤其在减小偏大的转向误差方面,O-CNOPs方法较BVs和SVs方法表现出了明显优势.尽管在台风转向角度预报中,O-CNOPs方法有较高的概率预报技巧,但其集合平均预报以及BVs、SVs集合平均预报的12h转向角度误差均大于控制预报.这可能是由于集合平均的滤波效应,导致集合平均预报的急

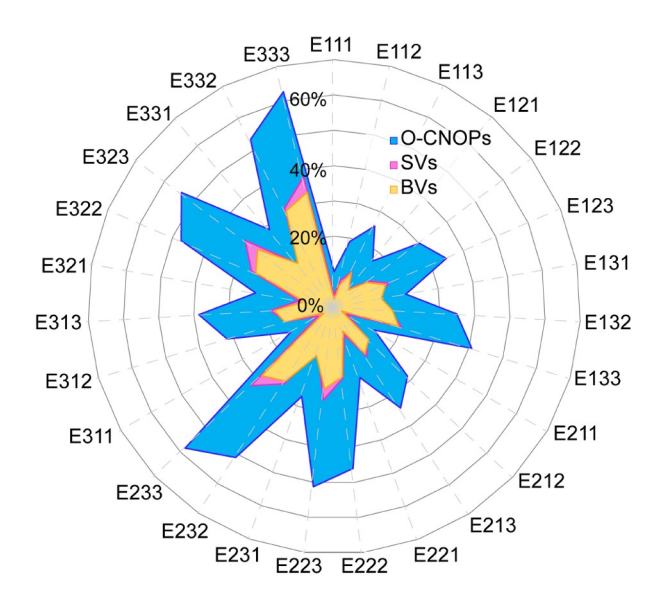


图 5 不同精度等级下,成功预报出台风急转向的集合成员 占总集合成员(483个)的比例

黄色、紫色和蓝色分别表示BVs、SVs和O-CNOPs集合预报; Eijk (i=1, 2, 3; j=1, 2, 3; k=1, 2, 3)表示由表2中第i个转向位置误差上限、第j个转向时间误差上限和第k个转向角度误差上限组合形成的精度等级

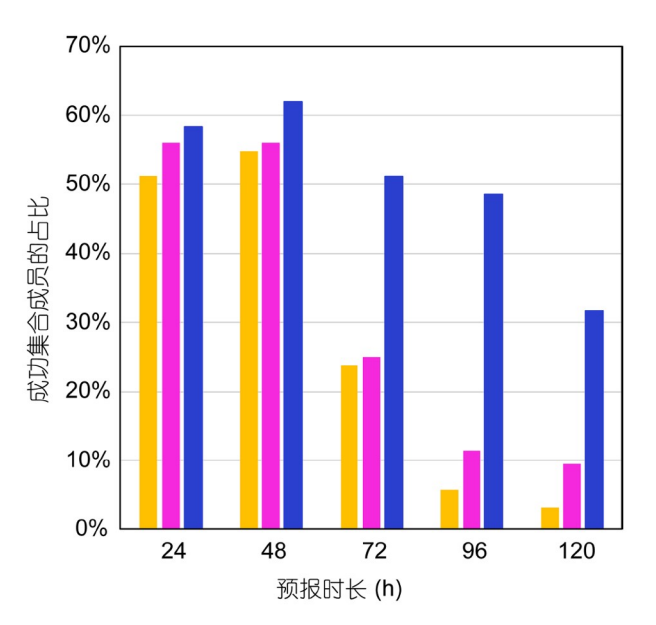


图 6 不同预报时效下,成功预报出台风异常转向的集合成员占总集合成员的比例

黄色、紫色和蓝色分别表示BVs、SVs和O-CNOPs集合预报;转向点、转向时间和转向角度的可接受误差上限为120km、12h和10°

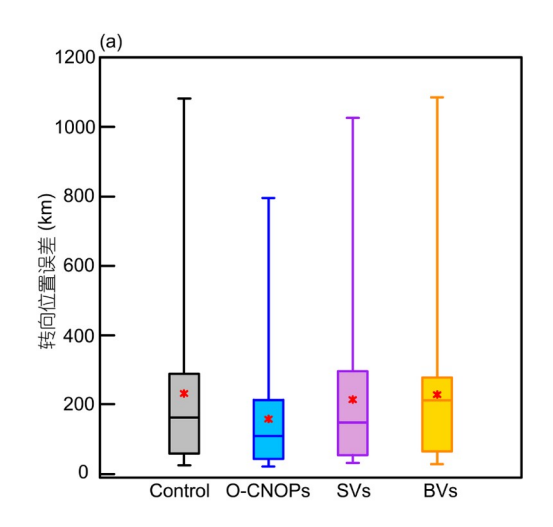
转弯角度与单个集合成员相比被过度平滑(见图2~图4). 此外, 钱奇峰和毛冬艳(2023)通过计算转向阶段的

路径预报误差,评估台风路径急转弯的预报技巧,基于 这一方法, 计算集合平均预报在转向阶段(转向前24h 至转向后24h)的路径误差. 图8通过箱型图展示了23次 预报中, 控制预报与三类集合平均预报的路径误差分 布情况, 结果表明: 随着台风临近转向, 控制预报的路 径误差呈上升趋势; SVs、BVs集合平均预报仅对控制 预报有微小改进, 路径预报误差的减少幅度均不足 3%; 相比之下, O-CNOPs集合平均预报在所有分位值 (25%、50%和75%)上均显著降低了路径预报误差. 统 计表明。在23次预报中、O-CNOPs集合平均预报将控 制预报的路径误差平均降低了29%以上. 对于路径误 差偏大的个例(定义为控制预报误差超过75%分位数 的样本), O-CNOPs的改进程度可达34%, 而SVs和BVs 的改进程度均不足2%. 此外, O-CNOPs方法具有最小 的四分位距(即上、下四分位数的间距), 这意味着O-CNOPs方法相较于SVs和BVs方法能够更稳定、更一 致地改进控制预报.

3.3 O-CNOPs集合成员更易再现台风急转向的物理原因

在表1列出的18个预报时段中,控制预报在台风"卡努"的第一个预报时段(起报时刻为2023年7月30日00时,即其路径发生东北向急转弯前约5天)路径预报误差最大.正如引言所述,台风"卡努"的东北向急转弯是业务预报的难点.对于这一疑难个例,只有O-CNOPs生成的集合成员能够明显偏离控制预报,其预报集合具有较大离散度并覆盖最佳路径,因而集合可靠性更高(见图2).本节以2023年7月30日00时起报的"卡努"路径集合预报试验为例,阐释为何O-CNOPs集合成员能够再现"卡努"的东北向急转弯,而SVs和BVs集合成员却难以实现.

三种方法的扰动湿能量(TMEs)的垂直结构不同(见图9). 在初始时刻, BVs的能量峰值出现在300hPa以上的高层大气, SVs的能量主要集中在800hPa以下的低层大气, 而O-CNOPs的能量在对流层中低层达到最大, 这与Zhang等(2023)的研究结果一致. 已有研究表明, 对流层中低层的初始不确定性对台风路径预报有重要影响(王晨稀和倪允琪, 2011; Torn等, 2018). 注意到, 仅有O-CNOPs有效识别出这一重要敏感区, 因此在不同高度上均能引发更大的TMEs增长(见图9). 因此, O-CNOPs更易生成偏离控制预报(未能捕捉"卡努"



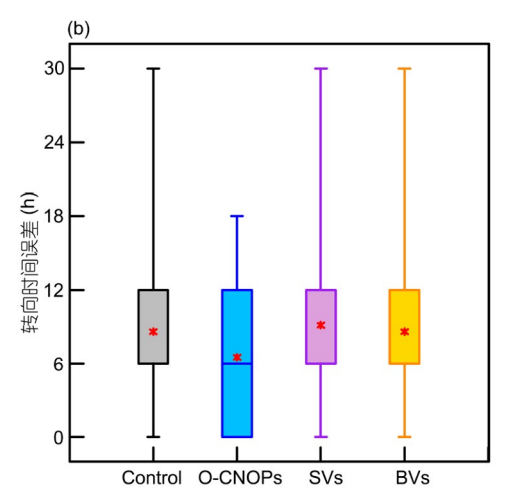


图 7 在23次预报中, 控制预报和集合平均预报的转向位置误差和转向时刻误差分布

(a、b)分别表示转向位置误差和转向时刻误差; 黑色、黄色、紫色和蓝色分别表示控制预报以及BVs、SVs和O-CNOPs集合平均预报; 红色点表示平均值, 箱型线给出了5%、50%和75%百分位值, 上、下横线表示除离群值之外的最大值和最小值

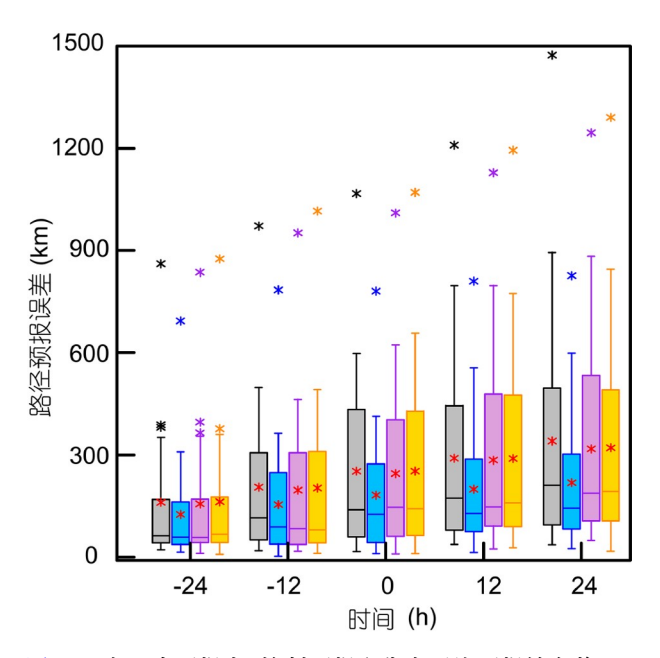


图 8 在23次预报中,控制预报和集合平均预报转向前24h 至转向后24h的路径误差分布

黑色、黄色、紫色和蓝色分别表示控制预报以及BVs、SVs和O-CNOPs集合平均预报; 红色点表示平均值, 其他点表示离群值, 箱型线给出了5%、50%和75%百分位值, 上、下横线表示除离群值之外的最大值和最小值

东北向急转弯)的集合成员, 其集合离散度更大, 从而更有可能成功捕捉台风路径的急转向(见图2).

图10给出了前三个BVs、SVs和O-CNOPs的水平 分布,以及控制预报在初始时刻的500hPa位势高度场

和引导气流. 受西北太平洋副热带高压(WPSH)的东南 引导气流影响,"卡努"早期向西北方向移动;随后,"卡 努"的异常路径与WPSH强度和位置的变化密切相关 (Chen等, 2024). 如图10所示, BVs的TMEs分散于台风 自身环流及其周围的大尺度环境场中; 而SVs与O-CNOPs的TMEs则更集中在WPSH与台风环流之间的 辐合区域. 不过, SVs和O-CNOPs的能量分布也存在差 异: SVs的TMEs主要位于"卡努"的西北侧,而O-CNOPs则呈现出围绕"卡努"附近的半环状结构。这意 味着、SVs和O-CNOPs均能识别WPSH对台风的重要 影响. 值得注意的是, O-CNOPs预报初期在"卡努"中 心附近及其周围的引导气流中产生的集合离散度远大 于SVs和BVs(见图11a)。这可归因于O-CNOPs的完全 非线性最优增长特性. O-CNOPs能够引发台风位置和 结构的显著调整,并通过台风与WPSH之间的动力相 互作用,影响WPSH的强度和位置,进而改变台风路径.

图12进一步展示了三类集合成员在500hPa位势高度场上5880-gpm等值线分布,以表征WPSH的结构特征.在O-CNOPs预报集合中,WPSH的强度和位置具有较大集合离散度(见图12a),尤其是在接近于"卡努"东北向急转弯的关键时段,体现了WPSH结构的预报不确定性;由于WPSH结构的多样性,其边缘引导气流具有较大集合离散度(见图11a),而该区域的引导气流正是决定"卡努"急转向的关键因子.因此,在台风转向位置和转向角度的预报中,O-CNOPs集合离散度更

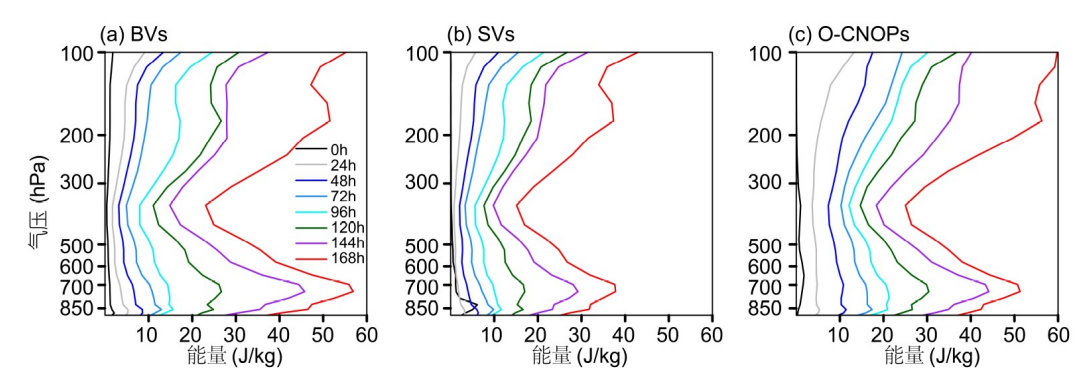


图 9 在2023年7月30日00时起报的"卡努"路径集合预报试验中, 扰动湿能量的垂直廓线

(a~c)分别表示BVs、SVs和O-CNOPs方法; 黑色线表示初始时刻, 不同彩色线分别表示24~168h预报时效; 扰动湿能量为整个模拟区域、所有集合成员平均的结果

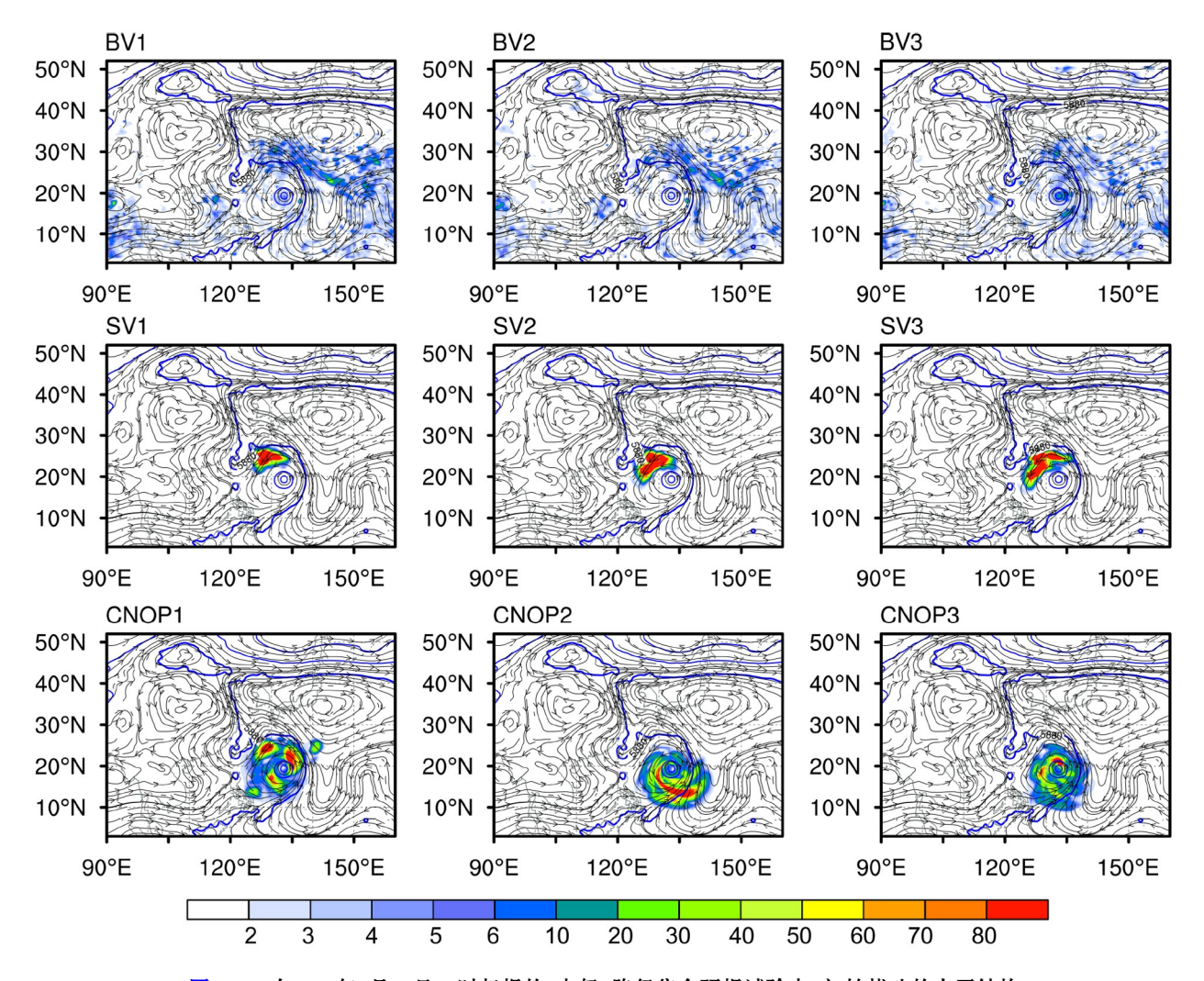


图 10 在2023年7月30日00时起报的"卡努"路径集合预报试验中, 初始扰动的水平结构

从上到下分别表示前三个BVs、SVs和O-CNOPs; 填色表示垂直平均的总湿能量(填色:单位: J/kg), 蓝色等值线表示500hPa位势高度场(单位: gpm), 黑色流线表示250~850hPa深层平均风(单位: m/s)

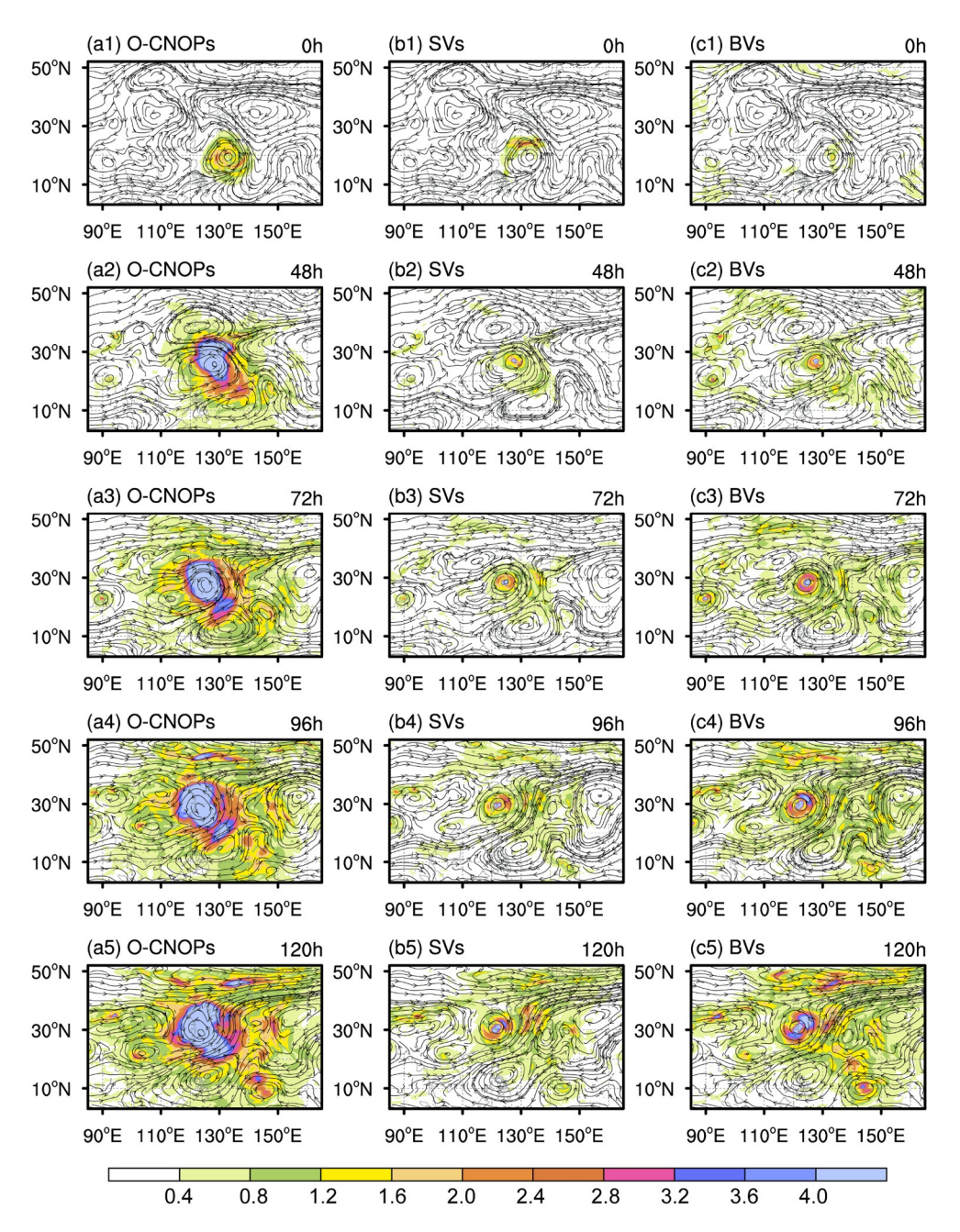


图 11 集合平均预报的250~850hPa深层平均风和其风速大小的集合离散度

(a~c)分别表示O-CNOPs、SVs和BVs方法; 从上到下分别表示起报时刻、48h、72h、96h和120h预报时效; 黑色流线表示深层平均风, 填色表示集合离散度(单位: m/s)

大(见图2). 相比之下, SVs和BVs预报集合中WPSH结构差异较小(见图12b和图12c), 台风周围引导气流的离散度更小(见图11b和图11c), 从而集合成员的路径预报集中在控制预报附近, 无法覆盖实际的转向位置和转向角度(见图2). 正如第3.2节所述, SVs和BVs均误

判"卡努"将在中国东部沿海登陆后东折,其转向角度远小于最佳路径.而O-CNOPs则更充分地表征了台风路径急转向过程中的不确定性,从而显著提升了成功捕捉台风路径急转弯的概率.

接下来,我们分析O-CNOPs方法在转向位置和转

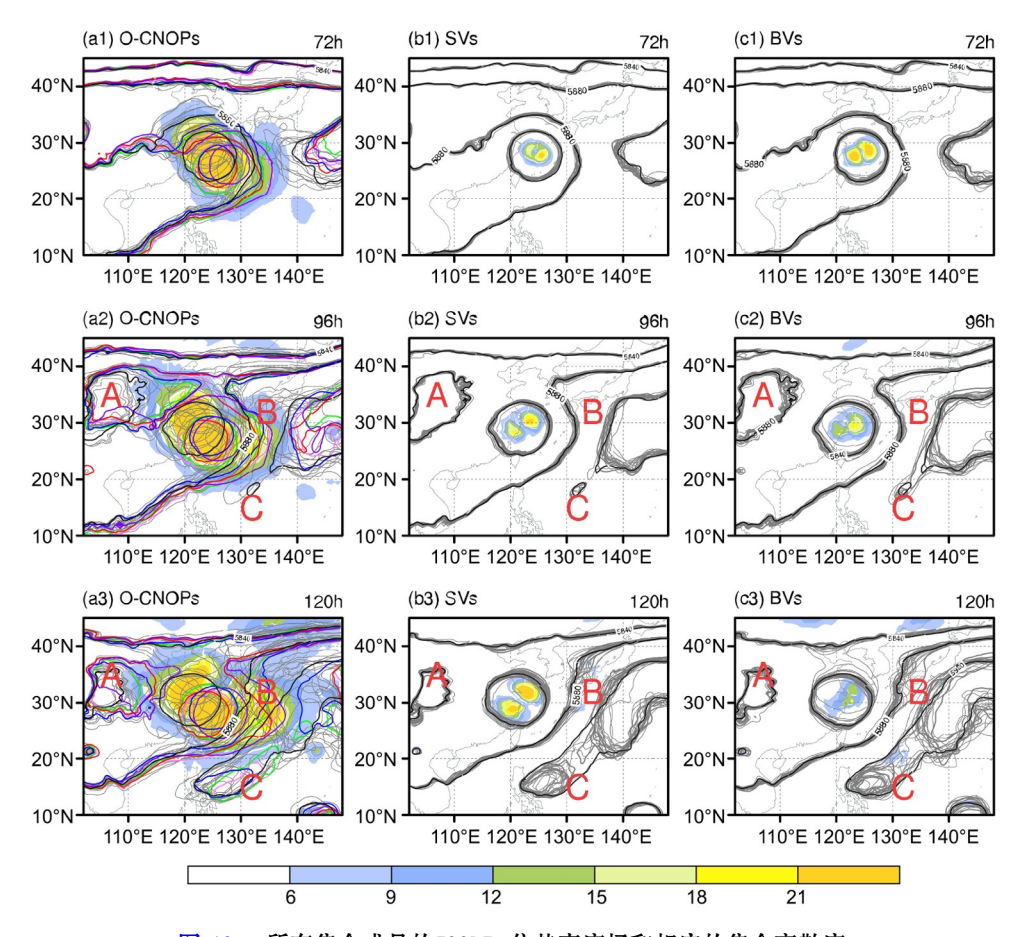


图 12 所有集合成员的500hPa位势高度场和相应的集合离散度

(a~c)分别表示O-CNOPs、SVs和BVs方法;从上到下表示72h、96h和120h预报时效;黑色等值线表示控制预报,彩色等值线表示成功预报出"卡努"东北向急转弯的5个O-CNOPs集合成员,灰色等值线表示其他集合成员

向角度预报中产生较大集合离散度的动力学机制.初始阶段,"卡努"受强大的WPSH引导向西北方向移动.在预报时效约为48h时,北侧WPSH迅速减弱,并在约96h时分裂为两个高压:一个位于台风西侧的弱副热带高压脊(图12中标记为A),另一个是位于台风东侧的副热带高压脊(即WPSH的主体,标记为B).此时,西侧高压脊产生的南向引导气流与东侧高压脊的北向引导气流相互抵消(见图11),台风周围引导气流减弱,其转向前移动速度明显减缓.在此阶段,O-CNOPs集合在"卡努"北侧呈现出较大集合离散度,表征了WPSH强度以及东、西高压脊位置的不确定性(见图12a2).这种不确定性直接影响西北向引导气流的强弱,进而调控台风在转向前西北行的速度.而转向前的移动速度又直接决定台风在西北方向所能到达的最远位置,即"卡努"的转向位置.在控制预报中,西侧高压脊过早减弱

并西撤(如图12中黑色等值线所示),造成西北向引导气流持续偏强,台风移动速度远快于最佳路径,导致转向位置预报明显偏西北.与BVs和SVs相比,O-CNOPs集合在转向前的移动速度上呈现出更大集合离散度,从而使"卡努"的转向位置具有更大集合离散度.在部分集合成员中,西侧高压脊维持较强(如图12a中的彩色等值线所示),有效减缓了台风西北行的速度,从而准确预报出实际转向位置.进一步地,台风南侧逐渐发展出一个反气旋系统(标记为C),其西北侧的西南气流增强,并与东侧高压脊西部的偏南气流汇合,迫使"卡努"在预报时效约120h时路径发生突变,转向东北方向移动.此时,O-CNOPs集合在台风南侧反气旋及东侧高压脊的强度和位置上表现出更大多样性(由图12a3中台风南侧至东侧的大离散度可见).不同的环境场配置能够影响引导气流中北向分量与西向分

量的相对强弱变化,进而影响台风转向后的移动方向及转向角度.在控制预报中,东侧高压脊过强造成北向引导气流被高估;同时南侧反气旋发展偏弱造成东南向引导气流被低估,使得控制预报错误地预测台风在转向后(120~144h)北上,未能再现"卡努"的东北向急转弯.然而,O-CNOPs集合中部分成员成功模拟出南侧反气旋较强、东侧高压脊较弱的环境场配置(如图12a中部分彩色等值线所示),有效修正了控制预报的转向角度偏差,成功再现了"卡努"转向后的东北行路径.

综上,O-CNOPs生成的集合成员能够有效表征台风引导气流的不确定性,进而通过台风与WPSH之间的相互作用过程影响台风转向.这使得O-CNOPs方法能够成功捕捉"卡努"的东北向急转弯,而SVs和BVs方法则难以实现.

4 总结和讨论

异常台风路径预报一直是业务预报的难点. 该研 究考察O-CNOPs方法在提高异常台风路径预报技巧 中的作用、将O-CNOPs方法和两种传统方法(SVs和 BVs)应用于WRF模式产生集合预报的初始扰动、对5 个具有异常路径的台风个例(即2010年台风"鲇鱼"、 2012年"天秤"、2022年台风"轩岚诺"、2023年台风 "卡努"和2023年台风"苏拉")开展了集合预报试验, 共 包括23个对台风转向预报的时段,基于集合预报结果, 首先对O-CNOPs、BVs和SVs方法的急转向预报能力 进行了概率评估. 结果表明, O-CNOPs方法能够更早 且具有更高概率地准确预报台风急转向,可为台风路 径突变提供更具价值的早期预警信息. 此外, O-CNOPs集合平均预报能够更稳定地提升台风异常转 向的预报技巧. 综合来看, 无论是确定性预报还是概率 预报、O-CNOPs在提高异常路径预报技巧方面都表现 出了明显优势.

以2023年台风"卡努"为例,该研究进一步揭示了O-CNOPs方法在台风异常转向预报中优于传统方法的物理原因。O-CNOPs能够更精准地识别台风运动较为敏感的中低层大气,以及台风环流附近关键的动力敏感区。由O-CNOPs最不稳定结构产生的集合成员,可通过台风与WPSH之间的动力相互作用过程,有效刻画与台风转向密切相关的引导气流不确定性,从而

成功捕捉"卡努"东北向急转弯的位置与角度.相比之下, SVs和BVs均未能充分刻画台风急转向过程中的不确定性, 因而其产生的集合成员均未能再现"卡努"的东北向急转弯. 更进一步, 从O-CNOPs产生的高质量集合预报资料中提取有用信息, 增强对台风异常运动形成机制的理解, 探究制约台风路径可预报性的关键因素, 为未来通过目标观测、模式改进等技术减少误差来源提供了潜在方向.

上述结果表明,O-CNOPs有潜力改进异常台风路径集合预报的可靠性. 但需要指出的是,对于某些台风个例,WRF模式采用的水平分辨率(30km)仍较为粗糙. 例如,O-CNOPs、BVs和SVs集合成员均未能再现2023年台风"苏拉"的打转路径,这可能是因为30-km分辨率无法充分解析小尺度台风的内部结构及其与环境场的复杂相互作用. 因此,提高模式分辨率是十分必要的,其面临的主要挑战之一是传统O-CNOPs求解算法所带来的高昂计算成本. 所幸, Ma等(2025)近期提出的并行迭代新算法可用于快速计算O-CNOPs,并基于理想模型验证了其在集合预报中的高效性与有效性. 若将该算法应用于高分辨率WRF模式,有望实时产生高技巧的台风路径集合预报. 此外,该高效算法还可拓展应用于台风强度、强降水以及其他高影响天气系统的对流尺度集合预报,具有广阔的业务应用前景.

目前,集合卡尔曼滤波(EnKF)资料同化方法已被 广泛应用于集合初始扰动构造,但它们的本质是资料 同化, 其优势在于能生成高质量初始场, 有效刻画观 测分布对初始不确定性的影响(Wang和Bishop, 2003; Ma等, 2008; Feng等, 2016), 但它产生的集合成员的离 散度往往偏小,导致预报不确定性被低估,通常需引入 膨胀系数进行修正(Yang等, 2015; Zheng和Zhu, 2016; Duan等, 2019; Li和Zhao, 2022). 该研究仅对比了O-CNOPs方法与基于误差动力增长理论的传统方法 (BVs和SVs), 未来需进一步系统分析O-CNOPs方法与 EnKF方法在台风路径集合预报中的表现差异. 除初始 误差外,模式误差对台风路径预报的影响也不可忽视. O-CNOPs仅考虑了初始不确定性,尽管其预报可靠性 优于传统方法, 但集合离散度-预报技巧关系(用于衡 量集合预报可靠性)仍不完美. 例如, 采用Zhang等 (2023)确定的试验配置、O-CNOPs倾向于高估台风路 径预报不确定性. Duan等(2022)的研究指出, 当预报系 统同时存在初始误差和模式误差时, 初始扰动与模式 扰动之间的动态协调增长可改进集合预报的可靠性.因此,发展并应用初始扰动与模式扰动的联合模态(例如Duan等(2022)提出的C-NFSVs方法),对于全面刻画初始与模式误差的综合影响、进一步改进集合预报的可靠性具有重要意义.

参考文献

- 戴高菊, 文永仁, 李英. 2014. 西北太平洋热带气旋运动及其突变的若干统计特征. 热带气象学报, 30: 23-33
- 聂高臻, 许映龙, 王海平. 2025. 2023年西北太平洋台风活动特征和 预报难点分析. 气象, 51: 369-381
- 钱奇峰, 毛冬艳. 2023. 2010-2019年ECWMF和NCEP集合模式对热带气旋路径预报的性能评估. 气象, 49: 224-234
- 王晨稀, 倪允琪. 2011. 影响热带气旋路径的敏感性试验与研究. 气象学报, 69: 757-769
- 向纯怡, 许映龙, 高拴柱, 王皘, 王海平. 2022. 2021年西北太平洋台 风活动特征和预报难点分析. 气象, 48: 1195–1208
- Birgin E G, Martínez J M, Raydan M. 2000. Nonmonotone spectral projected gradient methods on convex sets. SIAM J Optim, 10: 1196–1211
- Chan J C L, Li K K. 2005. Ensemble forecasting of tropical cyclone motion using a barotropic model. Part III: Combining perturbations of the environment and the vortex. Meteorol Atmos Phys, 90: 109– 126
- Chen R, Zhang W, Wang X. 2020. Machine learning in tropical cyclone forecast modeling: A review. Atmosphere, 11: 676
- Chen Y H, Sha S H, Lin C H, Hsiao L F, Huang C Y, Kuo H C. 2024.
 Performance evaluation of TGFS typhoon track forecasts over the western North Pacific with sensitivity tests on cumulus parameterization. Atmosphere, 15: 1075
- Cheung K K W. 2001. A review of ensemble forecasting techniques with a focus on tropical cyclone forecasting. Meteorol Appl, 8: 315–332
- Cheung K K W, Chan J C L. 1999. Ensemble forecasting of tropical cyclone motion using a barotropic model. Part I: Perturbations of the environment. Mon Weather Rev, 127: 1229–1243
- Conroy A, Titley H, Rivett R, Feng X, Methven J, Hodges K, Brammer A, Burton A, Chakraborty P, Chen G, Cowan L, Dunion J, Sarkar A. 2023. Track forecast: Operational capability and new techniques-summary from the tenth international workshop on tropical cyclones (IWTC-10). Tropical Cyclone Res Rev, 12: 64–80
- Diaconescu E P, Laprise R. 2012. Singular vectors in atmospheric sciences: A review. Earth-Sci Rev, 113: 161–175
- Duan W S, Huo Z H. 2016. An approach to generating mutually

- independent initial perturbations for ensemble forecasts: Orthogonal conditional nonlinear optimal perturbations. J Atmos Sci, 73: 997–1014
- Duan W S, Li X Q, Tian B. 2018. Towards optimal observational array for dealing with challenges of El Niño-Southern Oscillation predictions due to diversities of El Niño. Clim Dyn, 51: 3351–3368
- Duan W S, Ma J J, Vannitsem S. 2022. An ensemble forecasting method for dealing with the combined effects of the initial and model errors and a potential deep learning implementation. Mon Weather Rev, 150: 2959–2976
- Duan W S, Wang Y, Huo Z H, Zhou F F. 2019. Ensemble forecast methods for numerical weather forecast and climate prediction: Thinking and prospect (in Chinese). Clim Environ Res, 24: 396–406
- Dube A, Ashrit R, Kumar S, Mamgain A. 2020. Improvements in tropical cyclone forecasting through ensemble prediction system at NCMRWF in India. Tropical Cyclone Res Rev, 9: 106–116
- Feng J, Ding R Q, Li J P, Liu D Q. 2016. Comparison of nonlinear local Lyapunov vectors with bred vectors, random perturbations and ensemble transform Kalman filter strategies in a barotropic model. Adv Atmos Sci. 33: 1036–1046
- Gong Y, Li Y, Zhang D L. 2018. A statistical study of unusual tracks of tropical cyclones near Taiwan Island. J Appl Meteorol Climatol, 57: 193–206
- Huo Z H, Duan W S, Zhou F F. 2019. Ensemble forecasts of tropical cyclone track with orthogonal conditional nonlinear optimal perturbations. Adv Atmos Sci, 36: 231–247
- Lang S T K, Leutbecher M, Jones S C. 2012. Impact of perturbation methods in the ECMWF ensemble prediction system on tropical cyclone forecasts. Q J R Meteorol Soc, 138: 2030–2046
- Lei L, Ge Y, Tan Z M, Zhang Y, Chu K, Qiu X, Qian Q. 2022.
 Evaluation of a regional ensemble data assimilation system for typhoon prediction. Adv Atmos Sci, 39: 1816–1832
- Li Y, Heming J, Torn R D, Lai S, Xu Y, Chen X. 2023. Unusual tracks: Statistical, controlling factors and model prediction. Tropical Cyclone Res Rev, 12: 309–322
- Li Y, Zhao D. 2022. Climatology of tropical cyclone extreme rainfall over China from 1960 to 2019. Adv Atmos Sci, 39: 320–332
- Liu L, Feng J, Ma L, Yang Y, Wu X, Wang C. 2024. Ensemble-based sensitivity analysis of track forecasts of typhoon In-fa (2021) without and with model errors in the ECMWF, NCEP, and CMA ensemble prediction systems. Atmos Res, 309: 107596
- Lorenz E N. 1996. Predictability: A problem partly solved. Workshop on Predictability, Reading, United Kingdom, ECMWF, 1: 1–18
- Ma J J, Duan W S, Liu Z M, Wang Y. 2025. A new method to calculate nonlinear optimal perturbations for ensemble forecasting. Adv Atmos Sci, 42: 952–967

- Ma M, Peng M S, Li T, Wang L. 2022. Understanding the unusual track of Typhoon Lionrock (2016). Weather Forecast, 37: 393–414
- Ma X L, Xue J S, Lu W S. 2008. Preliminary study on ensemble transform Kalman filter-based initial perturbation scheme in GRAPES global ensemble prediction. Acta Meteorol Sin, 4: 526– 536
- Magnusson L, Doyle J D, Komaromi W A, Torn R D, Tang C K, Chan J C L, Yamaguchi M, Zhang F. 2019. Advances in understanding difficult cases of tropical cyclone track forecasts. Tropical Cyclone Res Rev, 8: 109–122
- Miller W, Zhang D L. 2019. Understanding the unusual looping track of hurricane joaquin (2015) and its forecast errors. Mon Weather Rev, 147: 2231–2259
- Miyachi T, Enomoto T. 2021. Tropical cyclone track forecasts using NCEP-GFS with initial conditions from three analyses. SOLA, 17: 140–144
- Palmer T. 2019. The ECMWF ensemble prediction system: Looking back (more than) 25 years and projecting forward 25 years. Q J R Meteorol Soc, 145: 12–24
- Pattanayak S, Mohanty U C. 2008. A comparative study on performance of MM5 and WRF models in simulation of tropical cyclones over Indian seas. Curr Sci, 95: 923–936
- Puri K, Barkmeijer J, Palmer T N. 2001. Ensemble prediction of tropical cyclones using targeted diabatic singular vectors. Q J R Meteorol Soc, 127: 709-731
- Qian W, Du J, Ai Y, Leung J, Liu Y, Xu J. 2024. Anomaly-based variable models: Examples of unusual track and extreme precipitation of tropical cyclones. Meteorology, 3: 243–261
- Skamarock W, Klemp J, Dudhia J, Gill D O, Barker D, Duda M G, Huang X Y, Huang W, Powers J G. 2008. A description of the advanced research WRF version 3. NCAR Technical Note, NCAR/ TN-475+STR
- Tang C K, Chan J C L, Yamaguchi M. 2021. Large tropical cyclone track forecast errors of global numerical weather prediction models in western North Pacific basin. Tropical Cyclone Res Rev, 10: 151– 169

- Thanh C, Tien T T, Chanh K Q. 2016. Application of breeding ensemble to tropical cyclone track forecasts using the Regional Atmospheric Modeling System (RAMS) model. Appl Math Model, 40: 8309–8325
- Torn R D, Elless T J, Papin P P, Davis C A. 2018. Tropical cyclone track sensitivity in deformation steering flow. Mon Weather Rev, 146: 3183–3201
- Toth Z, Kalnay E. 1993. Ensemble forecasting at NMC: The generation of perturbations. Bull Amer Meteorol Soc, 74: 2317–2330
- Toth Z, Kalnay E. 1997. Ensemble forecasting at NCEP and the breeding method. Mon Weather Rev, 125: 3297–3319
- Tseng J C H, Lai Y S. 2020. Perturbation structure and evolution in tropical cyclones Noul and Nepartak based on singular vectors. Tellus A-Dynamic Meteorol Oceanogr, 72: 1814589
- Wang X, Bishop C H. 2003. A comparison of breeding and ensemble transform Kalman filter ensemble forecast schemes. J Atmos Sci, 60: 1140–1158
- Yamaguchi M, Majumdar S J. 2010. Using TIGGE data to diagnose initial perturbations and their growth for tropical cyclone ensemble forecasts. Mon Weather Rev, 138: 3634–3655
- Yamaguchi M, Sakai R, Kyoda M, Komori T, Kadowaki T. 2009.
 Typhoon ensemble prediction system developed at the Japan Meteorological Agency. Mon Weather Rev, 137: 2592–2604
- Yang S C, Kalnay E, Enomoto T. 2015. Ensemble singular vectors and their use as additive inflation in EnKF. Tellus A-Dynamic Meteorol Oceanogr, 67: 26536
- Zhang X, Li Y, Zhang D L, Chen L. 2018. A 65-yr climatology of unusual tracks of tropical cyclones in the vicinity of China's coastal waters during 1949–2013. J Appl Meteorol Climatol, 57: 155–170
- Zhang H, Duan W S, Zhang Y C. 2023. Using the orthogonal conditional nonlinear optimal perturbations approach to address the uncertainties of tropical cyclone track forecasts generated by the WRF model. Weather Forecast, 38: 1907–1933
- Zheng F, Zhu J. 2016. Improved ensemble-mean forecasting of ENSO events by a zero-mean stochastic error model of an intermediate coupled model. Clim Dyn, 47: 3901–3915

(责任编委: 雷荔傈)